Supplement of Atmos. Chem. Phys., 22, 10077–10097, 2022
https://doi.org/10.5194/acp-22-10077-2022-supplement
© Author(s) 2022. CC BY 4.0 License.

Atmospheric Chemistry and Physics
Open Access
EGU

Supplement of

Seasonal variation in oxygenated organic molecules in urban Beijing and their contribution to secondary organic aerosol

Yishuo Guo et al.

Correspondence to: Chao Yan (chaoyan@nju.edu.cn)

The copyright of individual parts of the supplement might differ from the article licence.

Section S1. Determination of Original OOM Molecule

In the measurement of nitrate CIMS, one OOM molecule (X) could be detected as deprotonated ion (X^-), adduct with NO_3^- ($X•NO_3^-$) or adduct with $HNO_3•NO_3^-$ ($X•HNO_3NO_3^-$). The acidity of OOM molecules is not very strong so that they hardly exist in de-protonated ions. In Ehn et al., by using isotopically labeled nitric acid ($H^{15}NO_3$) as the reagent, it was found that OOMs mainly existed as adducts with NO_3^-, and to a lesser extent with $HNO_3NO_3^-$ (Ehn et al., 2014). This is because the binding energy of OOMs with NO_3^- is smaller than with $HNO_3NO_3^-$ (Hyttinen et al., 2015).

Besides, the evidence that most OOMs cluster with NO_3^- could also be found from the time variations of corresponding OOMs. As shown in Fig. S1, the time variations of $C_7H_{10}O_5NO_3^-$ and $C_7H_{11}O_8NNO_3^-$ are not consistent, indicating that they are different OOMs charged both by NO_3^-, instead of the same OOM charged by NO_3^- and $HNO_3NO_3^-$, respectively. This is also the same for other OOMs, such as $C_8H_{12}O_5NO_3^-$ and $C_8H_{13}O_8NNO_3^-$.

From the above discussion, we know that OOM molecules are primarily detected as clusters with NO_3^-. ($X•NO_3^-$). Therefore, the original formula of a detected ion Y could be obtained based on the following criteria:

a. If there is no nitrogen atom in Y, it is treated as a deprotonated species.

b. If there is at least one nitrogen atom in Y, it is treated as an adduct with NO_3^-.

Section S2. Definition of Oxygenated Organic Molecules (OOMs)

The terminology OOMs comes from the term HOMs (Highly Oxygenated Organic Molecules), which is defined based on three criteria (Bianchi et al., 2019): a. HOMs are formed via autoxidation involving peroxy radicals, b. HOMs are formed in the gas phase under atmospherically relevant conditions, and c. HOMs typically contain six or more oxygen atoms. However, when looking into the oxygenated organic molecules measured at urban Beijing, the criteria of a. and c. are not always met. For example, in the oxidation processes, precursor VOCs may undergo multi-generation oxidation (Zaytsev et al., 2019;Garmash et al., 2020) and the autoxidation is sometimes suppressed by high NO_x level. This leads to the fact that not all organic molecules measured by nitrate CIMS contain six or more oxygen atoms (see Fig. S7). This is the reason why we didn't use the term HOMs.

OOMs is a more general terminology that refers to the gas phase organic compounds which are formed via oxidation process under atmospheric conditions. Thus, the guidelines for the classification of OOMs should be:

a. OOMs are the gas-phase oxygen-containing organic molecules detected under atmospherically relevant conditions.

b. OOMs can be formed via oxidations in the gas phase, heterogeneous reactions on aerosol surface, or evaporated processes from aerosols.

Section S3. Estimation of OOM Volatility

Detailed structure information of OOMs in real atmosphere is still unknown, therefore, the volatility of each OOM molecule was estimated based on a parameterization using numbers of different atoms (Donahue et al., 2011). For the oxidation products from monoterpenes, previous studies show that except from hydroxyl (-OH), carbonyl (=O) and carboxyl (-O(=O)H) groups, hydroperoxide (-OOH) also takes a large portion (Tröstl et al., 2016;Stolzenburg et al., 2018). Then by assuming that all nitrogen atoms exist as organonitrate groups ($-ONO_2$), the saturation mass concentration of OOM molecule at 300 K can be given as follows (Mohr et al., 2019):

$$\log_{10}C^*(300K) = (25 - nC)\cdot bC - (nO - 3nN)\cdot bO - 2 * \left[\frac{(nO - 3nN)\cdot nC}{nC + nO - 3nN}\right]\cdot bCO - nN\cdot bN \quad (1)$$

where nC, nO and nN are the numbers of carbon, oxygen, and nitrogen in each molecule respectively, and bC=0.475, bO=0.2, bCO=0.9, and bN=2.5. For oxidation products from aromatics, the work of Wang et al. shows that they possess more hydroxyl and carbonyl groups as well as less hydroperoxides, and that their estimated saturation concentrations suggested by Donahue et al. (Donahue et al., 2011) match well with the experiment ones (Wang et al., 2020). Therefore, for those non-monoterpene OOMs, the estimation from Donahue et al. was applied:

$$\log_{10}C^*(300K) = (25 - nC)\cdot bC - nO_{eff}\cdot bO - 2 * \left(\frac{nC\cdot nO_{eff}}{nC + nO_{eff}}\right)\cdot bCO \quad (2)$$

where nC, nO_{eff} and nN are the numbers of carbon, effective oxygen and nitrogen in each molecule separately, and bC=0.475, bO=2.3, and bCO=-0.3.

The temperature dependence of C^* is given by the Clausius-Clapeyron equation (Epstein et al., 2010;Donahue et al., 2012), which we can be approximated as:

$$\log_{10}C^*(T) = \log_{10}C^*(300K) + \frac{\Delta H_{vap}}{R\ln(10)}\left(\frac{1}{300} - \frac{1}{T}\right) \quad (3)$$

where the evaporation enthalpy ΔH_{vap} can be linked with $\log_{10}C^*(300K)$ according to the following equation:

$$\Delta H_{vap}[kJ\ mol^{-1}] = -5.7\cdot\log_{10}C^*(300K) + 129 \quad (4)$$

After the temperature related saturation concentrations were calculated, OOMs were then grouped into different bins based on the volatility basis set (VBS) (Donahue et al., 2006), and further classified as ELVOCs (extremely low volatility organic compounds), LVOCs (low volatility organic compounds), SVOCs (semi-volatile organic compounds), IVOCs (intermediate volatility organic compounds) and VOCs (volatile organic compounds) according to their volatilities (Donahue et al., 2012).

Section S4. Uncertainty Discussion on OOM Volatility Estimation

The derived OOM volatility may vary among different methods. Volatility parameterization based on numbers of different atoms originated from the work of Donahue (Donahue et al., 2011). This study gave a good volatility estimation for OOMs which only contain carbon, hydrogen and nitrogen atoms, and meet the requirements of containing mostly hydroxyl, carbonyl and carboxyl groups and possessing equal fraction of hydroxyl and carbonyl.

With deeper understanding of monoterpene oxidation mechanism during the past decade, many studies have found that hydroperoxide is also a key functional group of monoterpene oxidation products (Ehn et al., 2014;Jokinen et al., 2014;Praplan et al., 2015;Berndt et al., 2016). Based on the proposed structures of those products, the group-contribution method SIMPOL could be applied to calculate the volatilities of monoterpene-derived OOMs. And the results were further used for revising the original volatility parameterization (Tröstl et al., 2016;Stolzenburg et al., 2018;Mohr et al., 2019;Bianchi et al., 2019). And therefore, the volatility estimation of monoterpene OOMs based on Eq. 1 should be pretty robust and has the least uncertainty compared with other types of OOMs.

For aromatic OOMs, the volatility estimation according to Eq. 2 was also evaluated by Wang et al. (Wang et al., 2020). In this work, the oxidation experiments of toluene and naphthalene by OH radical were performed under

conditions similar to typical urban environments. Results showed that this equation works well for toluene dimers, naphthalene monomers and naphthalene dimers, while overestimates the volatility a little bit for toluene monomers. In our study, it is likely that most aromatic OOMs are in the form of monomers. And thus, the values of $\log_{10}C^*$ for aromatic OOMs derived from Eq. 2 might be overestimated slightly.

The chemical pathways of atmospheric isoprene oxidation have been investigated for years. Early studies showed that carbonyl, hydroxyl and organonitrate groups are the main functional groups of isoprene OOMs (Lee et al., 2014;Schwantes et al., 2015). In recent years, some studies found that hydroperoxide could also be formed through the process of intramolecular H-shift (Wang et al., 2018b;Zhao et al., 2021;Wu et al., 2021). However, different from the stable hydroperoxides on monoterpene OOMs, some hydroperoxides on isoprene OOMs are unstable and may undergo fragmentation (Teng et al., 2017). Besides, this formation of hydroperoxides tend to occur under low-NO_x or experimentally design conditions (D'Ambro et al., 2017;Zhao et al., 2021;Wu et al., 2021). Therefore, the fraction of hydroperoxide groups on isoprene OOMs could not be taken directly from experimental results. Fortunately, the work of Xu et al. (Xu et al., 2021) provided us valuable information of observed isoprene OOMs in Nanjing, one of the Chinese megacities. Results showed that there is large fraction of organonitrate groups and probably small fraction of hydroperoxide groups for isoprene OOMs formed under megacity atmosphere. And this is reason why we didn't apply the volatility parameterization from monoterpene OOMs, which contain large fraction of hydroperoxides, to isoprene OOMs. In addition, the work of Wu et al. (Wu et al., 2021) estimated the volatility of isoprene nitrates by comparing the difference between two sets of experiments with and without seed aerosol addition. But as seed aerosols inevitably brought in heterogeneous reactions on the surface and liquid phase reactions in the particle phase, this method seems not suitable for volatility acquisition. Future thermal desorption experiments like the one conducted by Wang et al. (Wang et al., 2020) may give better estimation.

For aliphatic OOMs, direct volatility parameterization has been lacking, and only few studies proposed its formation pathways. Conventional knowledge suggests that the oxidation products from alkanes as well as alkenes mainly contain carbonyl, hydroxyl and organonitrate groups (Ziemann, 2011), while possibilities still remain for the formation of hydroperoxides (Rissanen et al., 2014;Rissanen, 2018;Wang et al., 2021). Yet, the lack of mechanism on aliphatic OOM formation under urban-related atmospheric conditions hampers the understanding of aliphatic OOM structures. Thus we are not able to decide whether Eq. 1 or Eq. 2 is more suitable for them.

To solve this problem, we calculated aliphatic OOM volatility with both methods the results were summarized in Fig. S2. Although some difference appears for detailed volatility distribution, the concentrations of condensable aliphatic OOMs (ELVOCs and LVOCs) based on Eq. 1 and Eq. 2 are very consistent. And therefore, the contribution of aliphatic OOMs to SOA condensation growth will not be influenced too much by the method chosen. In this study, we finally use Eq. 2 to calculate the volatility of aliphatic OOMs.

Section S5. Simulation of OOM Net Condensation Flux

An aerosol growth model was used to calculate the OOM net condensation flux onto particles (Tröstl et al., 2016;Stolzenburg et al., 2018). This model is based on the VBS distribution mentioned above, and each VBS bin is regarded as a single surrogate species with the averaged mass and concentration.

The condensation flux, $\emptyset_{i,p}$, of low volatile OOMs at each moment can be simulated as:

$$\emptyset_{i,p} = N_p \cdot \sigma_{i,p} \cdot k_{i,p} \cdot F_{i,p}$$

where N_p, $\sigma_{i,p}$, $k_{i,p}$ and $F_{i,p}$ are the particle number concentration at a given size (p), the particle-vapor collision cross-section between each VBS bin (i) and a given particle size (p), the deposition rate of OOM vapor at the particle surface, and the driving force of condensation respectively. $\sigma_{i,p}$ is derived from the particle diameter d_p and vapor diameter d_i as:

$$\sigma_{i,p} = \pi/4(d_p + d_i)^2$$

The deposition rate of OOMs, $k_{i,p}$, depends on the center mass velocity of particle and vapor $v_{i,p}$, the mass accommodation coefficient $\alpha_{i,p}$, and the non-continuum dynamic factor $\beta_{i,p}$:

$$k_{i,p} = \alpha_{i,p} v_{i,p} \beta_{i,p}$$

where $v_{i,p} = \sqrt{\frac{8RT}{\pi \mu_{i,p}}}$, is the average velocity for Maxwell's velocity distribution law. $\mu_{i,p}$ is the reduced mass and is defined as $\frac{M_i M_p}{M_i + M_p}$.

The driving force of condensation is defined as:

$$F_{i,p} = C_i^0 (S_i - a'_{i,p})$$

where C_i^0, S_i and $a'_{i,p}$ are the saturation vapor concentration, saturation ratio and particle phase activity of each VBS bin, respectively. The excess saturation ratio $S_i^{XS} = S_i - a'_{i,p}$ is the key diagnostic for condensation. $a'_{i,p}$ accounts for particle mixture effect with Raoult term $X_{i,p}\gamma_{i,p}$ and curvature effect with Kelvin term $K_{i,p}$ as:

$$a'_{i,p} = X_{i,p} \gamma_{i,p} K_{i,p}$$

where $X_{i,p}$ is the mass fraction of organic compounds of each VBS bin (i) in the condensed phase at given particle size (p), and $\gamma_{i,p}$ is the mass based activity coefficient in the condensed phase. In this study, $\gamma_{i,p} = 1$ was used with the assumption of ideal solution. The Kelvin term, $K_{i,p} = \exp\left(\frac{4\sigma_p M_i}{RT\rho_p D_p}\right)$, is related to surface tension σ_p, molar weight M_i and density ρ_p.

For OOMs with relatively higher volatility (i.e., C_i^*>0.1 μg m^{-3}), their partitioning between the gas and condensed phase will likely reach equilibrium when the condensation and evaporation of OOMs are approximately equal. Then the fraction of species i in condensed phase, f_i^{aer}, can be described by the aerosol partition theory (Seinfeld and Pandis, 2016) as:

$$f_i^{aer} = \frac{1}{1 + C_i^*/C_{OA}^{aer}} = \frac{C_i^{aer}}{C_i}$$

where C_i^*, C_i, C_{OA}^{aer}, and C_i^{aer} are the effective saturation concentration of the OOMs vapor in each VBS bin, total mass concentration of species i in the gas and condensed phase, total mass concentration of organic aerosol, and mass concentration of species i in the condensed phase.

The seasonal variations of OOM condensation fluxes for low volatility OOMs (ELVOCs and LVOCs) and high volatility OOMs (SVOCs, IVOCs and VOCs) are shown in Fig. S3 (A) and (B) respectively. It can be found that, compared with low volatility OOMs, the condensation flux of high volatility OOMs is minor, and the net flux of them onto particles are zero over a period of time. Consequently, the rate of OOMs condensing onto particles could be approximately estimated based on the condensation of ELVOCs and LVOCs.

According to the above model, the condensation flux is mainly influenced by the oversaturation of OOMs and the surface area of aerosols ($Area_{aero}$). Since ELVOCs and LVOCs undergo almost irreversible condensation (Ehn et al., 2014), their gas phase concentration is nearly the same as their oversaturated concentration. Therefore, we further looked into the relationship between condensation flux and ELVOC and LVOC concentration ([ELVOCs+LVOCs]) times $Area_{aero}$. Results in Fig. S4 show that they have perfect linear correlation in all four seasons. The slope in the figure represents the ability of ELVOCs and LVOCs forming SOA through condensation, to be more specific, the amount of SOA produced through condensation by unit concentration of ELVOCs and LVOCs (1 $\mu g/m^3$) under unit aerosol surface concentration (1 m^2/m^3) in an hour. This condensation ability of ELVOCs and LVOCs is quite stable during the year (6.3-8.4 $m^2 \cdot m^{-3} \cdot h$). And its influencing factors are possibly particle composition, concentration of gaseous vapors and the interaction between vapors and particle surface.

Section S6. Definition of Characteristic Accumulation Time

The characteristic accumulation time (AccTime), which is introduced for roughly comparison of SOA formation rates from OOM condensation among different seasons, is defined as:

$$\mathrm{AccTime} = \frac{[\mathrm{SOA}]}{[\mathrm{CondenFlux}]_{\mathrm{ELVOC+LVOC}}}$$

where [SOA] is the mass concentration of SOA in $\mu g \cdot m^{-3}$, and $[CondenFlux]_{ELVOC+LVOC}$ is the mass condensation flux of OOMs in $\mu g \cdot m^{-3} \cdot h^{-1}$, and therefore, AccTime is in the unit of hour.

In real atmosphere, there are various SOA sources. So this AccTime should not be interpreted as that SOA is entirely formed from OOM condensation within this characteristic time, but only a straightforward estimation of how fast SOA is formed if its source only comes from OOM condensation.

FIGURES

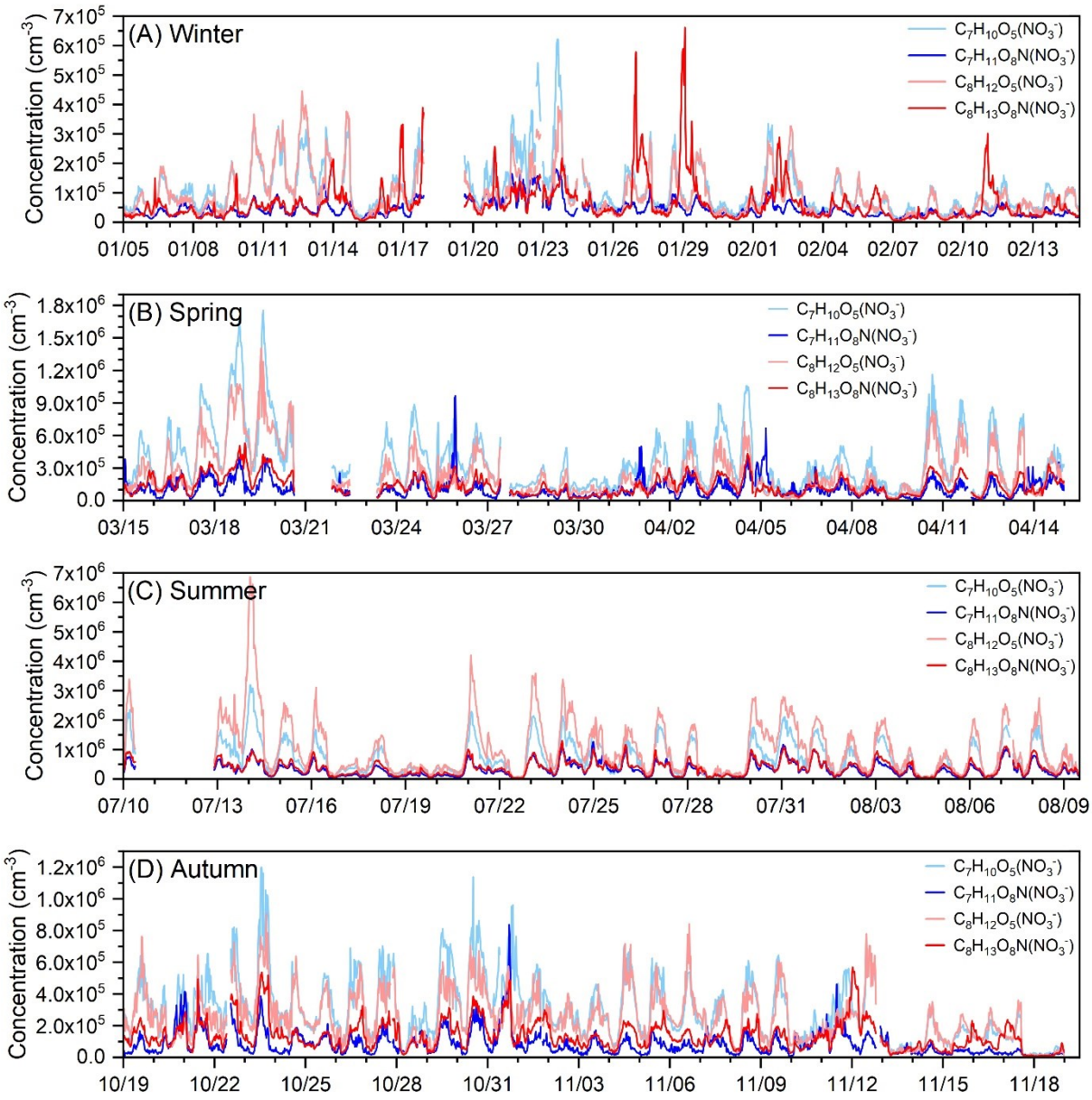

Figure S1. The time variations of $C_7H_{10}O_5(NO_3^-)$, $C_7H_{11}O_8N(NO_3^-)$, $C_8H_{12}O_5(NO_3^-)$ and $C_8H_{13}O_8N(NO_3^-)$ during four seasons.

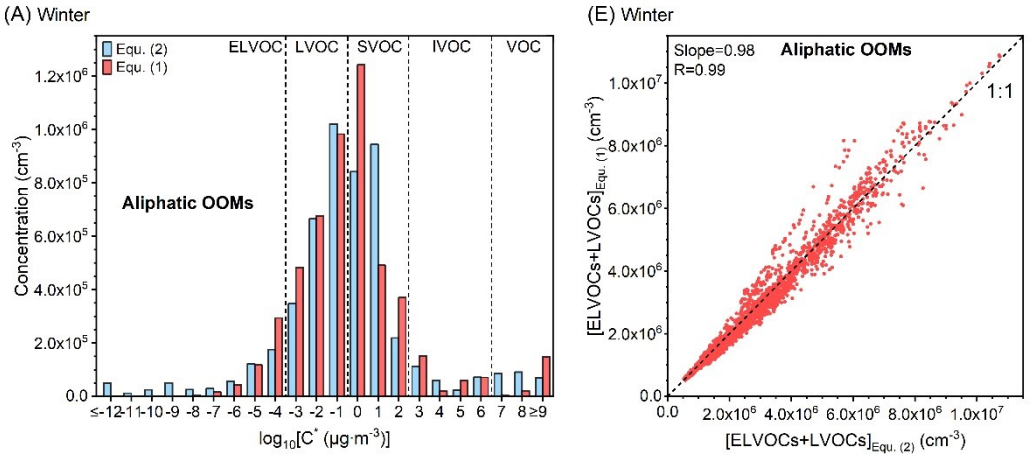

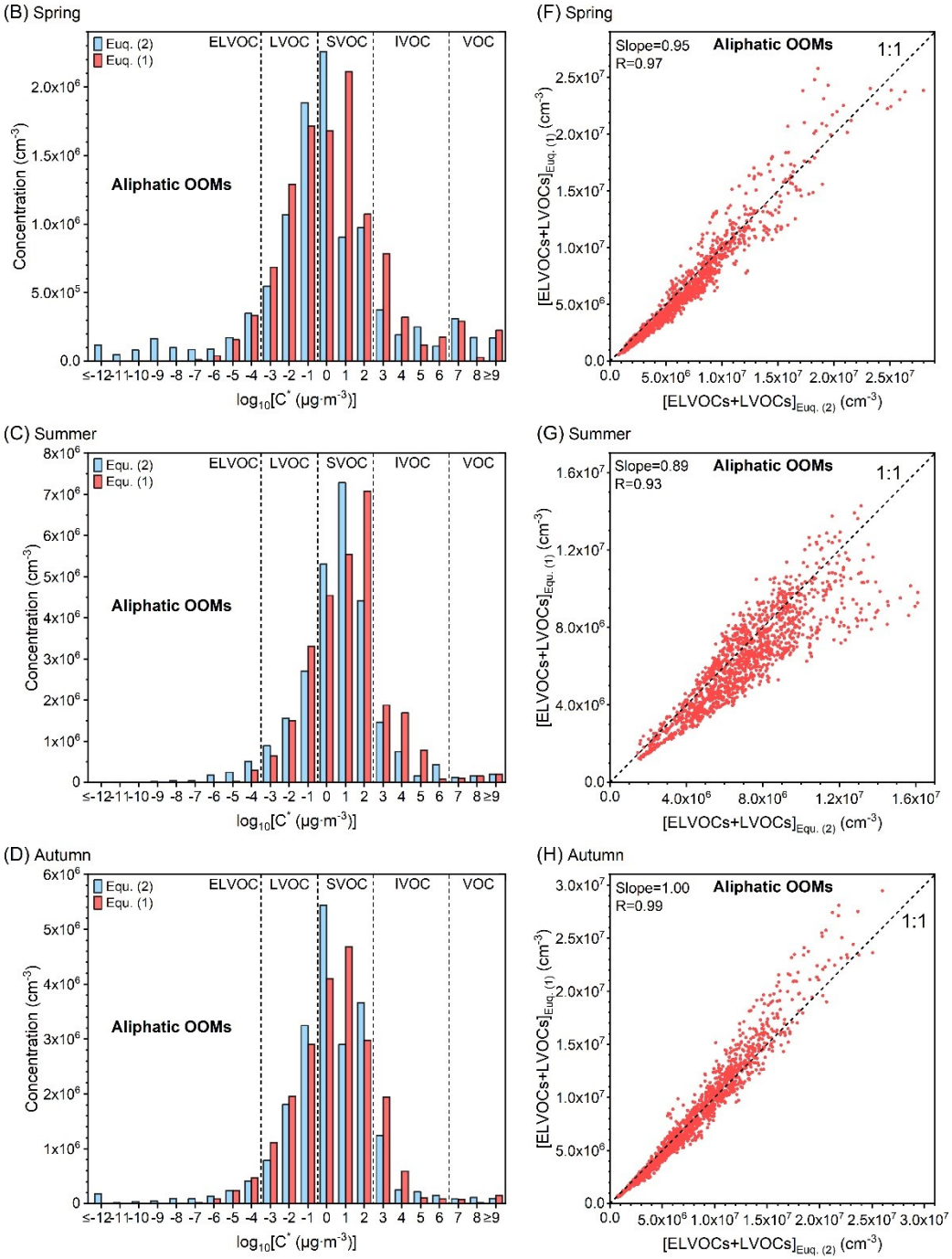

Figure S2. (A) - (D) Estimated aliphatic OOM volatility distribution derived from two parameterization methods for four season. **(E) - (F)** Comparison of aliphatic OOM concentrations belonging to ELVOCs and LVOCs between two parameterization methods for four seasons. In Fig. (E) to (F), the slopes of least-square linear fit and Pearson coefficients are also listed.

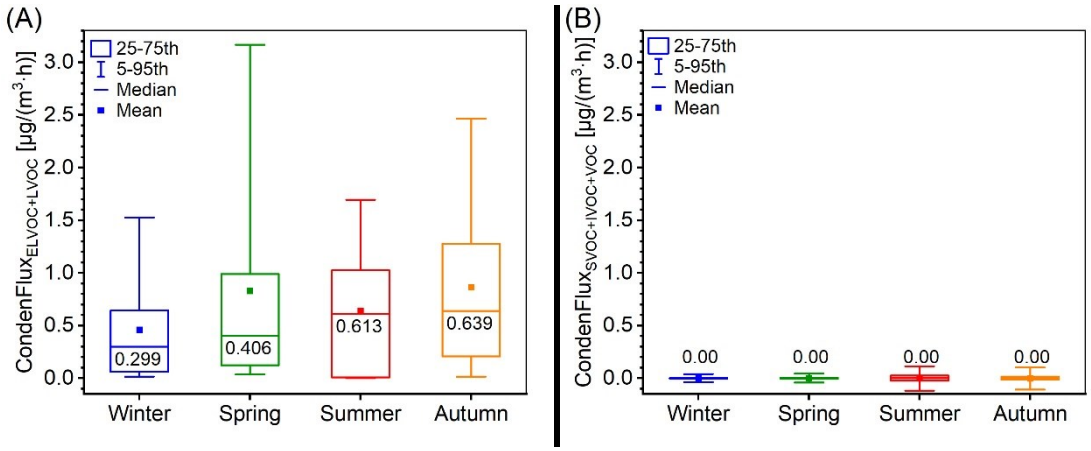

Figure S3. Condensation fluxes of (A) low volatility OOMs (ELVOCs and LVOCs) estimated by the particle dynamic model (Tröstl et al., 2016), and (B) high volatility OOMs (SVOCs, IVOCs and VOCs) calculated based on the aerosol partition theory (Seinfeld and Pandis, 2016) in four seasons**.** The values in each box are the median values.

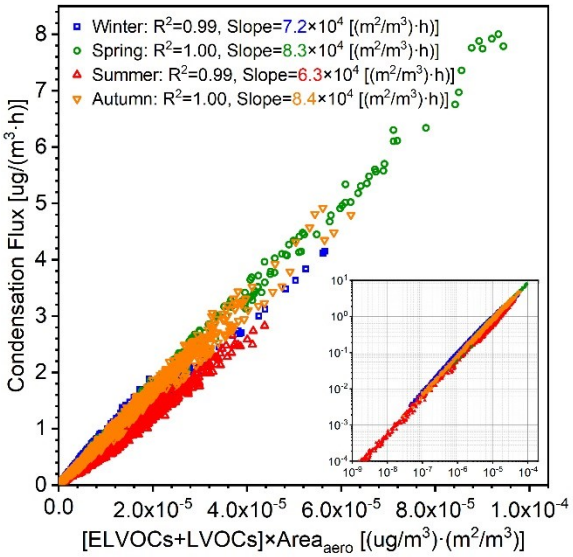

Figure S4. Relationship between OOM condensation flux and concentration of ELVOCs and LVOCs ([ELVOCs+LVOCs]) times aerosol surface area (Area$_{aero}$). The figure inserted is in log scale.

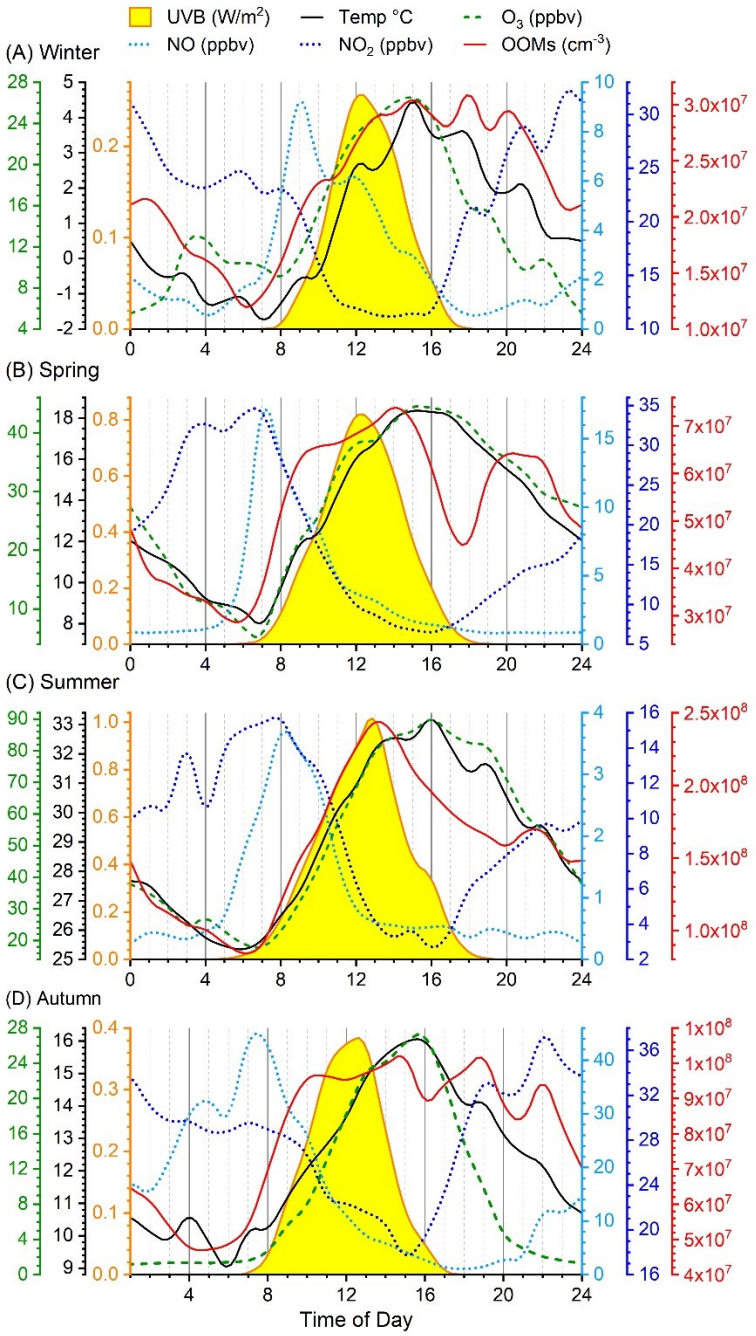

Figure S5. Diurnals variations of UVB, temperature (Temp), mixing ratio of O_3, NO and NO_2, and OOM concentration in four seasons.

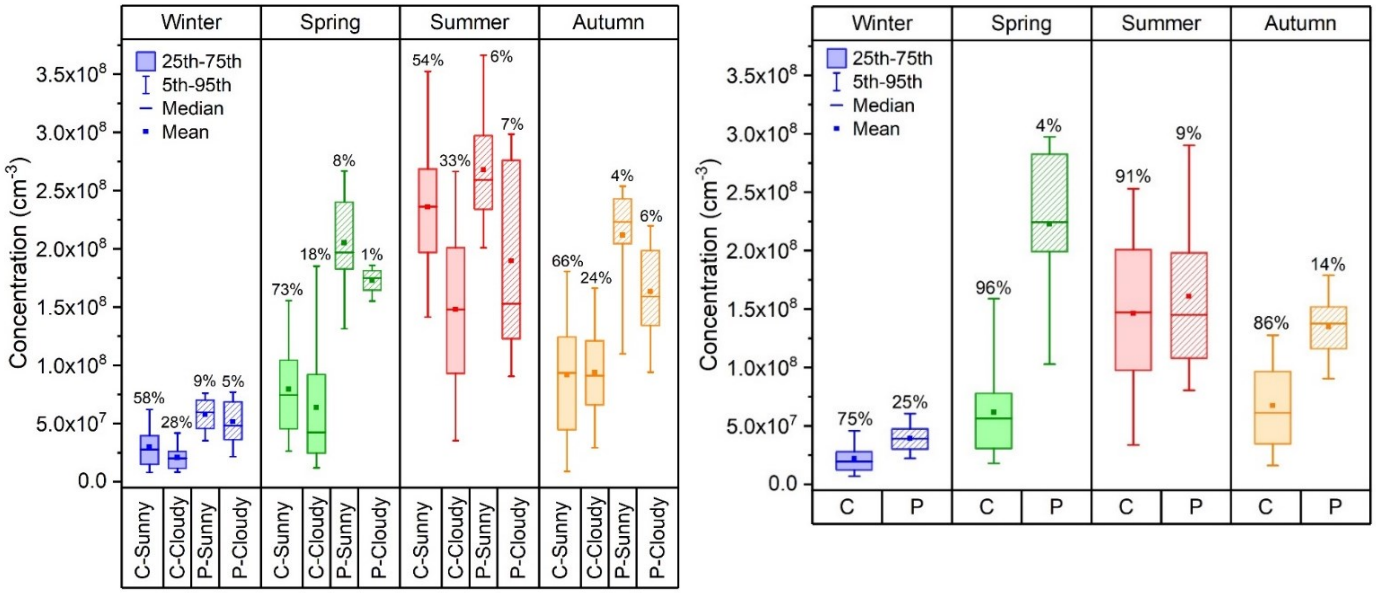

Figure S6. Left panel: Concentration of total OOMs in four seasons under different atmospheric conditions during daytime (08:00-16:00). The abbreviations "C" and "P" represent clean and polluted condition respectively. Clean and polluted conditions are divided by $PM_{2.5}$ with a value of 75 μg/m^3. Sunny and cloudy day are distinguished by brightness parameter (Dada et al., 2017) with a value of 0.5. The percentages are fractions taken up by each condition in each season. Right panel: Concentration of total OOMs in four seasons under different atmospheric conditions during nighttime (20:00-04:00 next day). The abbreviations "C" and "P" represent clean and polluted respectively. Those two conditions are divided by $PM_{2.5}$ with a value of 75 μg/m^3. The percentages are fractions taken up by each condition in each season.

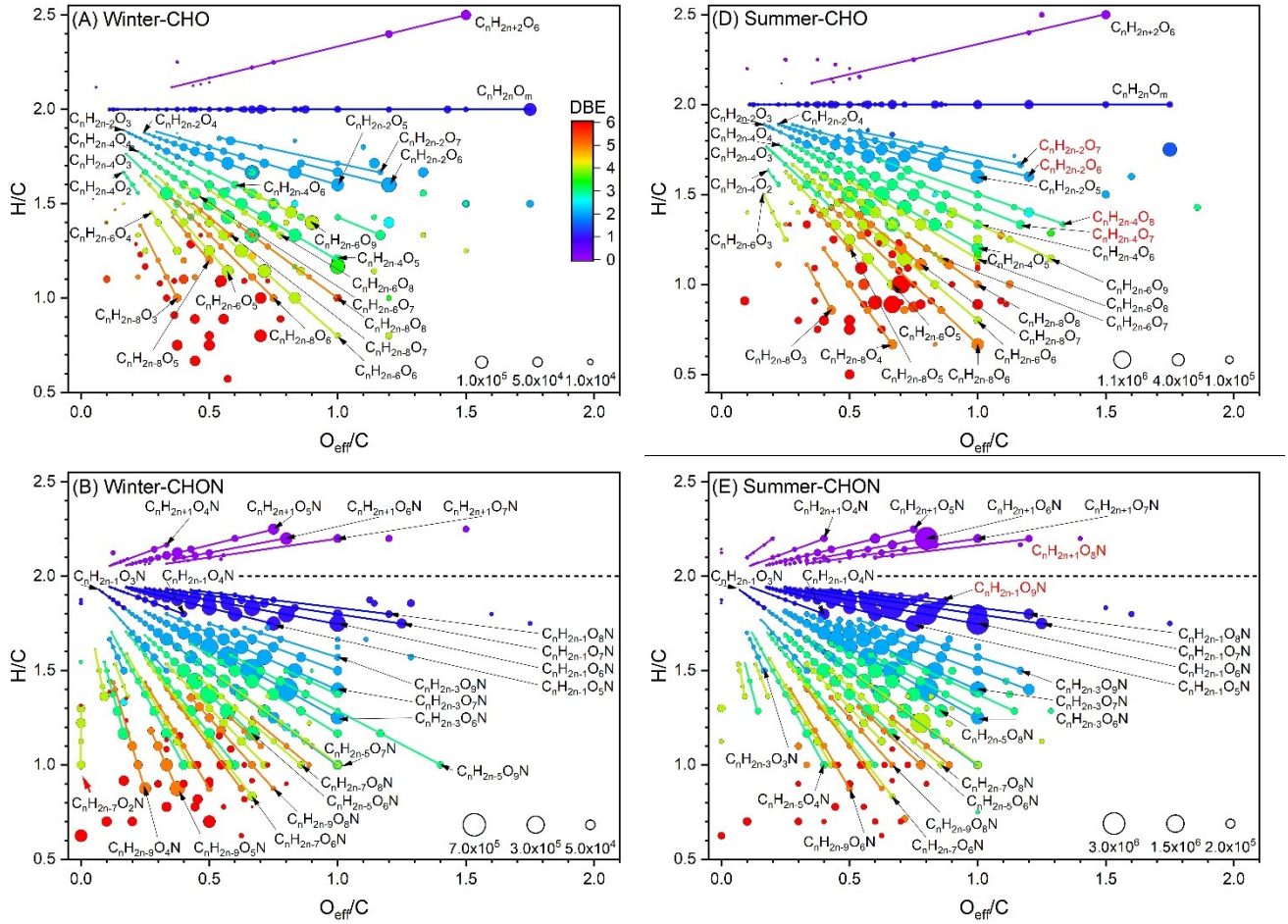

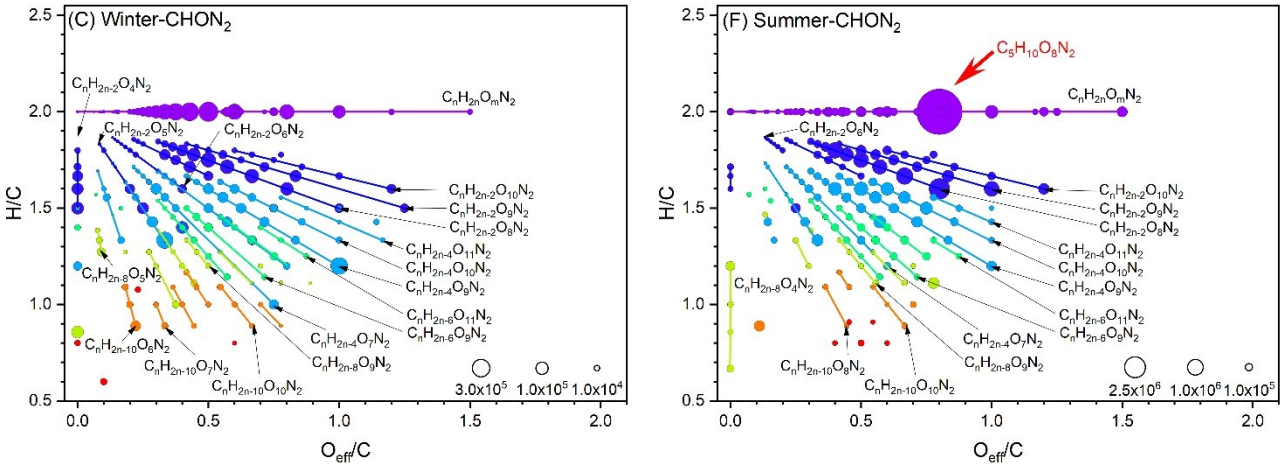

Figure S7. The ratio of hydrogen number to carbon number (H/C) against the corresponding ratio of effective oxygen number to carbon number (O_{eff}/C) for **(A)** winter CHO OOMs, **(B)** winter CHON OOMs, **(C)** winter $CHON_2$ OOMs, **(D)** summer CHO OOMs, **(E)** summer CHON OOMs, and **(F)** summer $CHON_2$ OOMs. The size relates to the concentration of each OOMs molecules. CHO OOMs are those only contain carbon, hydrogen and oxygen atoms. CHON OOMs and $CHON_2$ OOMs are those contain additional one and two nitrogen atoms respectively.

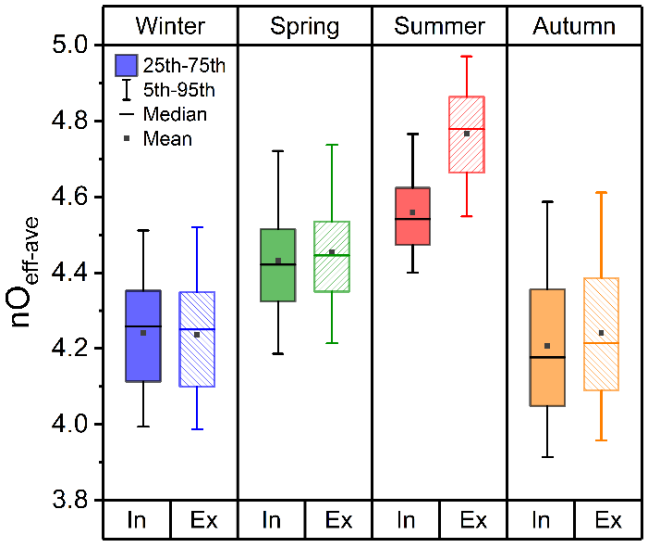

Figure S8. Concentration weighted average number of effective oxygen ($nO_{eff\text{-}ave}$) in four seasons. The abbreviations "In" and "Ex" represent the averaged values for OOMs with and without IP-derived OOMs respectively.

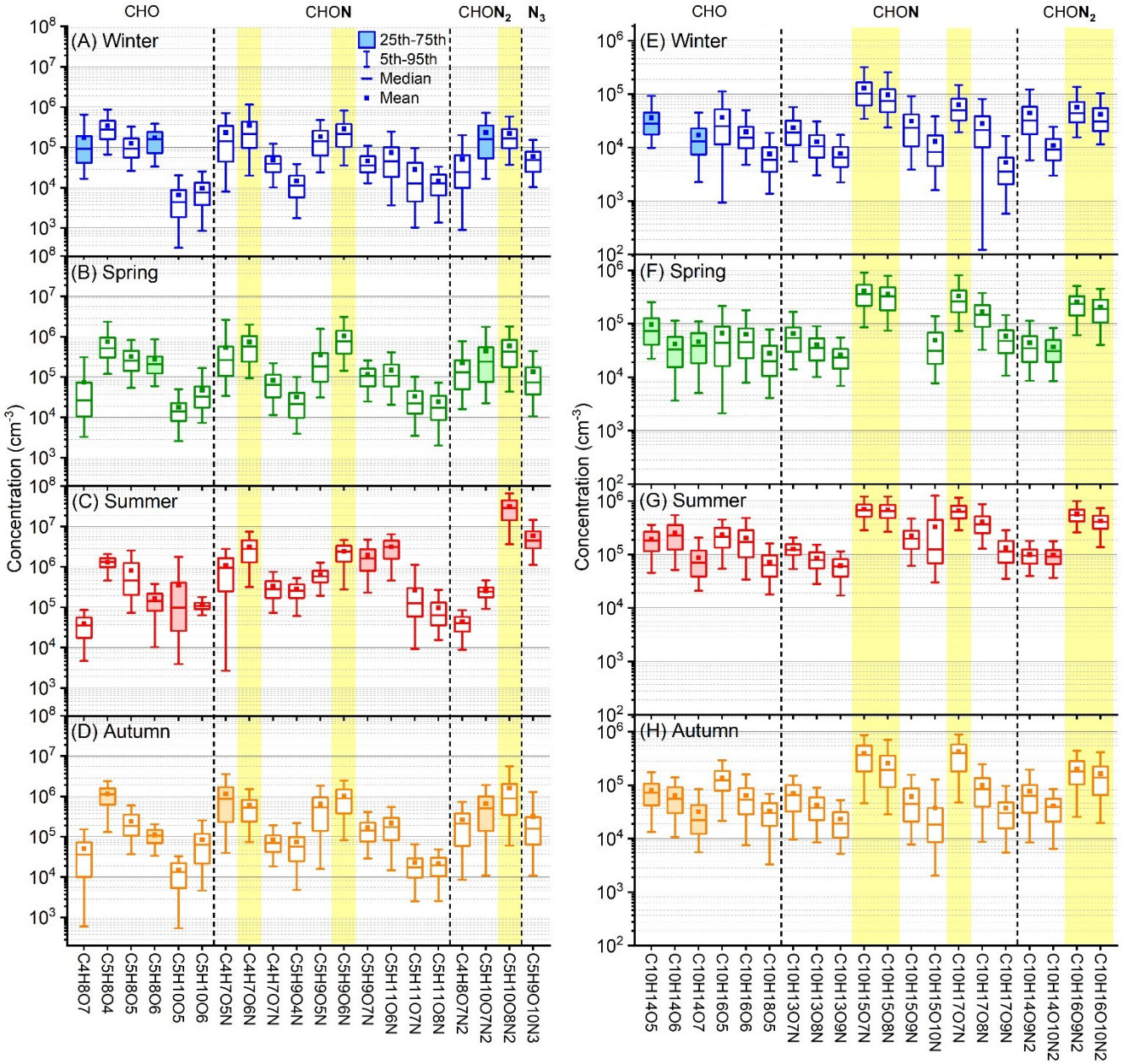

Figure S9. Concentration of typical IP OOMs in (A) winter, (B) spring, (C) summer and (D) autumn, and typical MT OOMs in (E) winter, (F) spring, (G) summer and (H) autumn. Species in grey background are distinct ones in different seasons. Compounds in yellow background are primary ones during the year. The filled boxes are special compounds in each season.

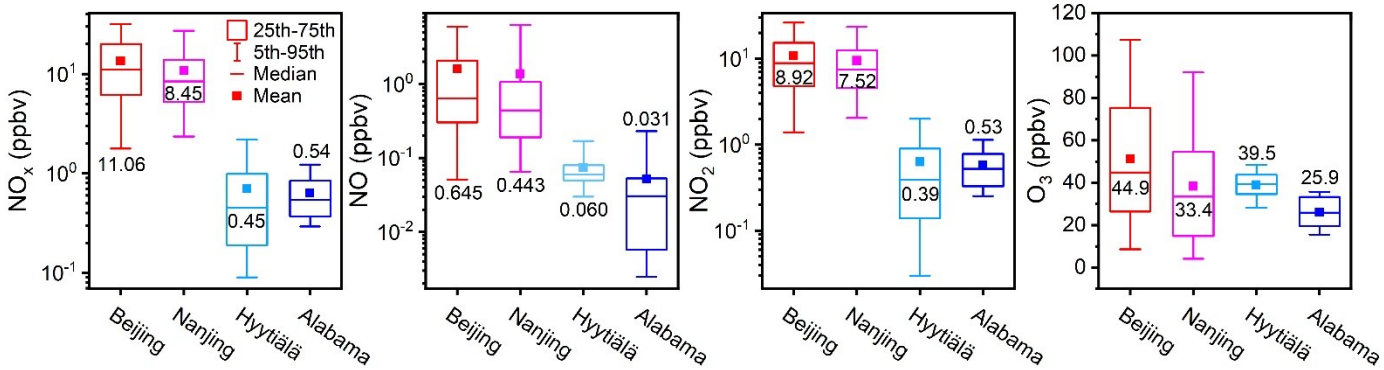

Figure S10. NO_x, NO, NO_2 and O_3 mixing ratios in summer Beijing, summer Nanjing (Liu et al., 2021) , spring Hyytiälä (Yan et al., 2016) and summer Alabama (Massoli et al., 2018).

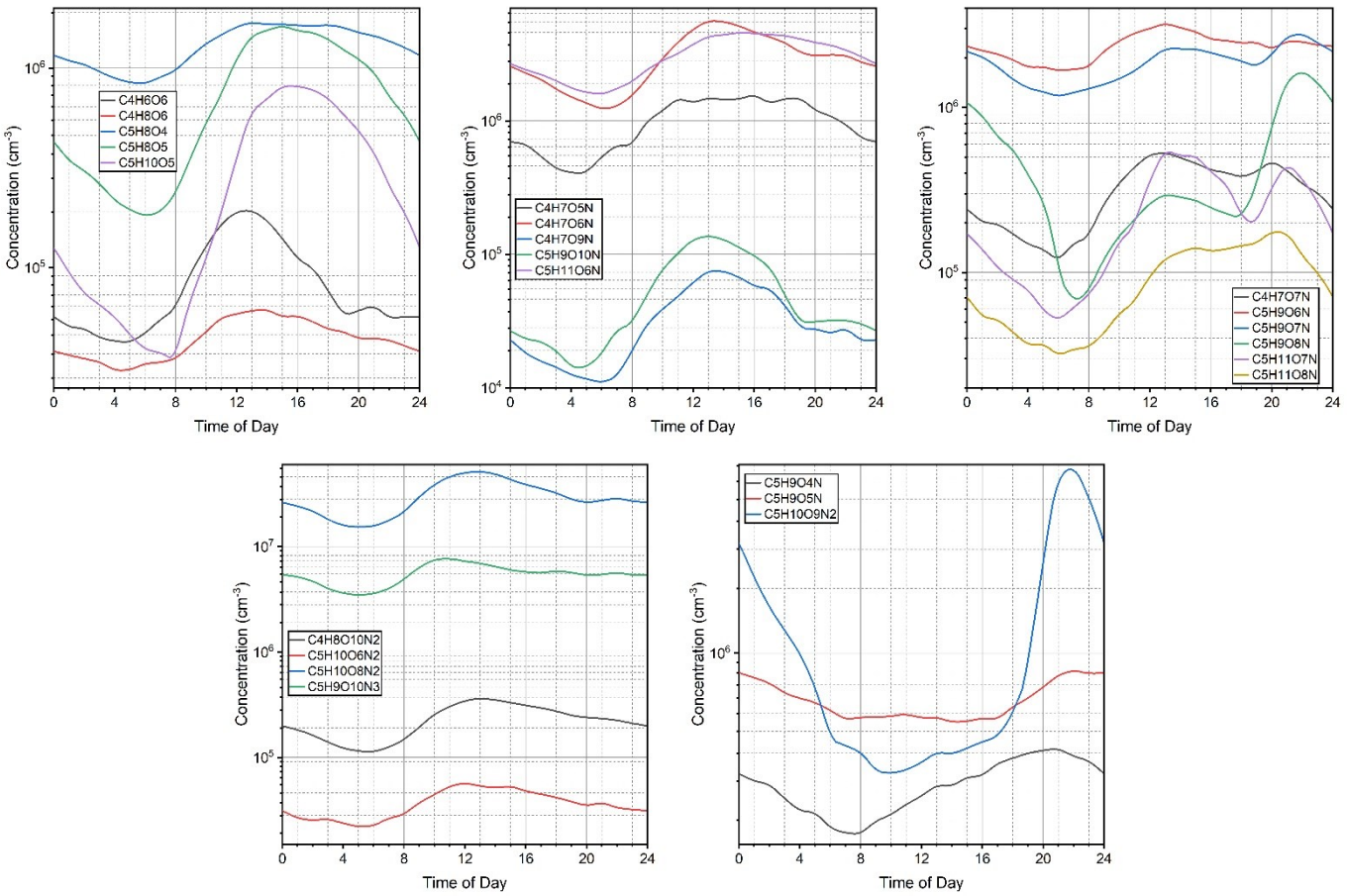

Figure S11. Diurnal variations of representative isoprene OOMs during summertime in this study.

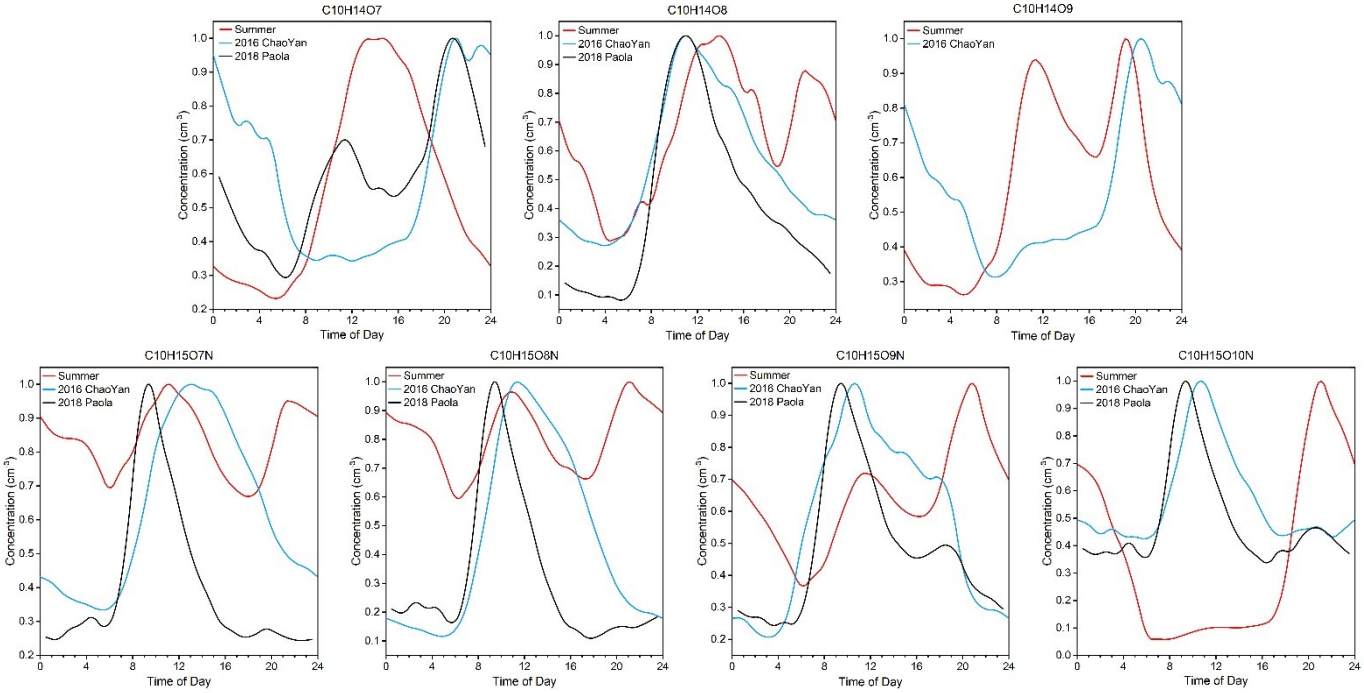

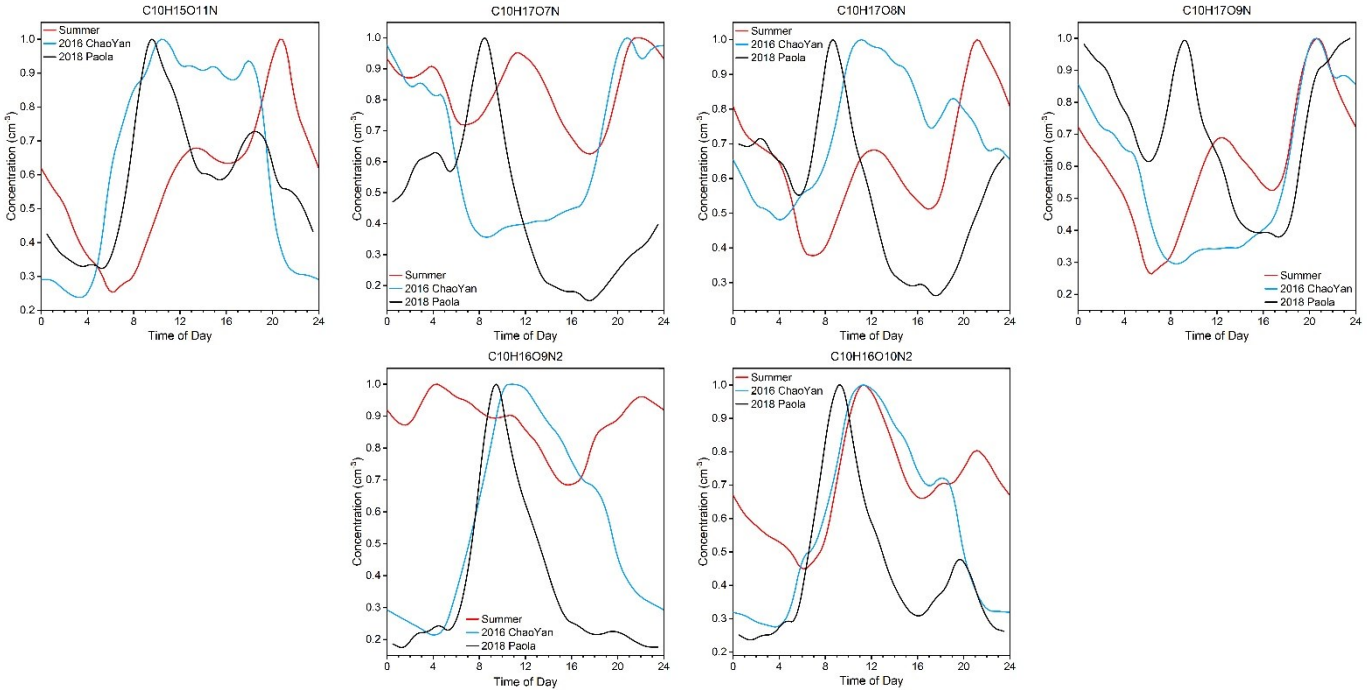

Figure S12. Diurnal variation of representative monoterpene OOMs during summertime in our study and from other two reported forest sites (Yan et al., 2016;Massoli et al., 2018).

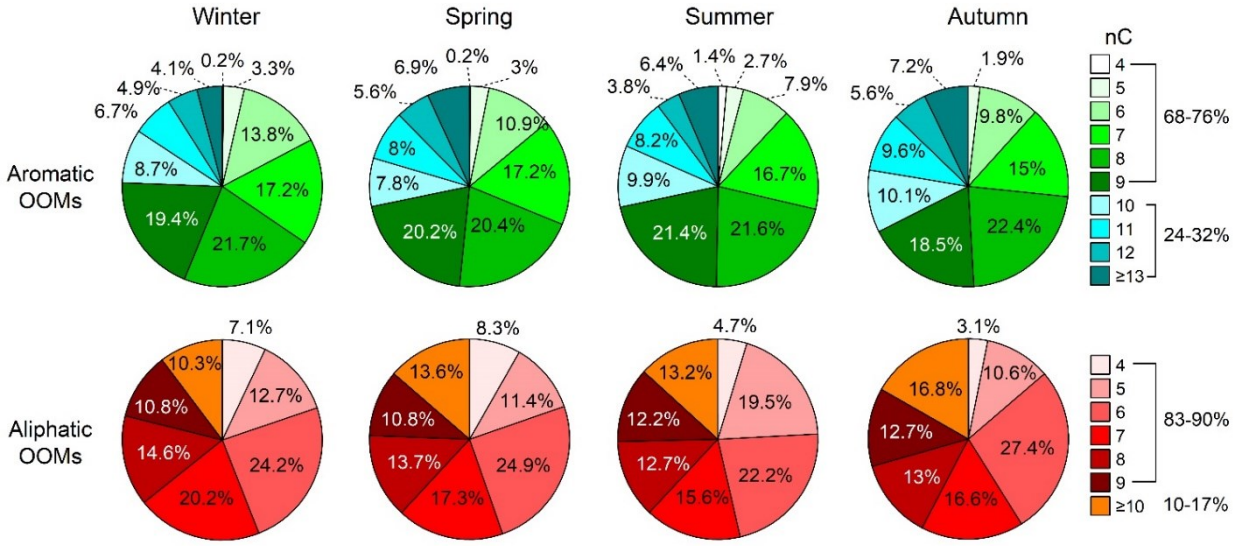

Figure S13. Fractions of aromatic (first row) and aliphatic (second row) OOMs with different number of carbon atoms (nC) in winter (first column), spring (second column), summer (third column) and autumn (forth column). Colors in green, blue, red and orange series are for monocyclic aromatic OOMs (nC≤9), polycyclic aromatic OOMs (nC≥10), short-chain aliphatic OOMs (nC≤9) and long-chain aliphatic OOMs (nC≥10) respectively.

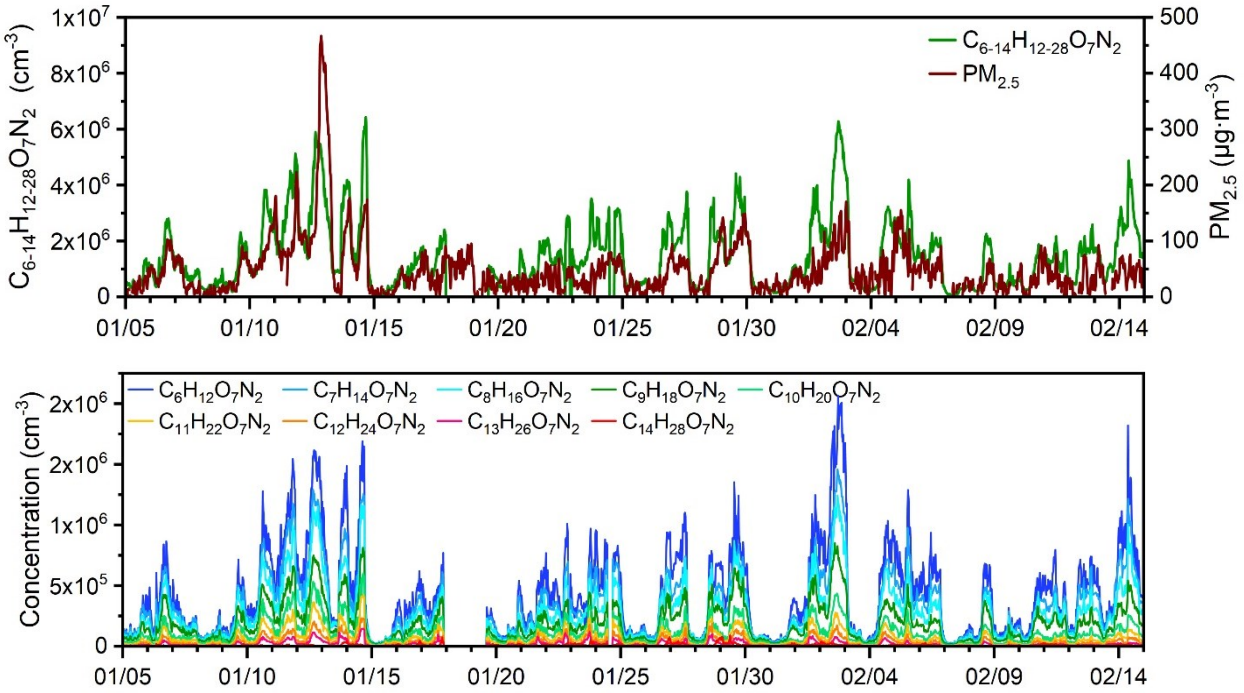

Figure S14. Time variation of $C_{6-14}H_{12-28}O_7N_2$ OOMs and $PM_{2.5}$ in winter.

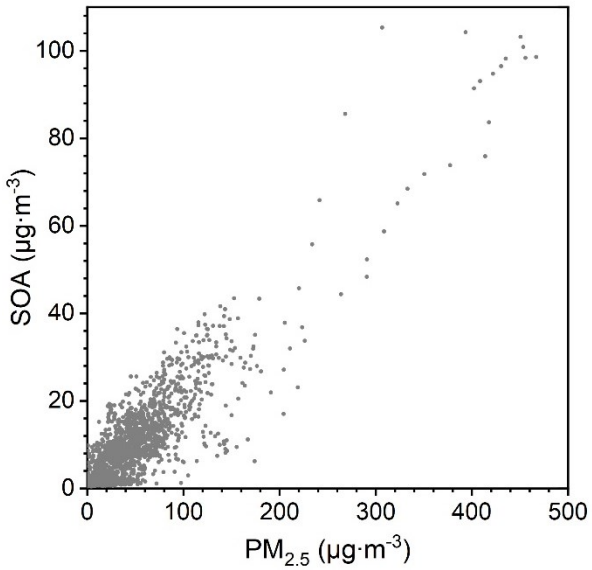

Figure S15. Correlation of SOA with $PM_{2.5}$ in winter.

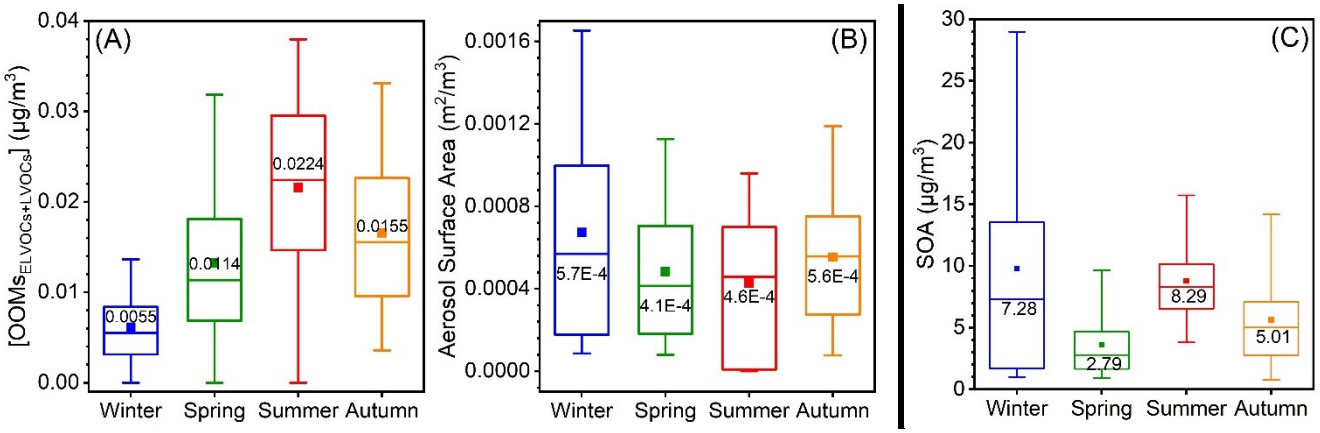

Figure S16. (A) Mass concentration of ELVOCs and LVOCs, (B) aerosol surface area in four seasons and (C) mass concentration of secondary organic aerosol (SOA) in four seasons. The values in each box are the median values of corresponding parameters.

TABLES

Table S1. Median values of UVB, temperature (Temp), relative humidity (RH), O_3, NO, NO_2, condensation sink (CS), organic aerosol (OA) and secondary organic aerosol (SOA) in four seasons. Please note that note that UVB only includes daytime values from 08:00 to 16:00.

Median Values	UVB (W/m^2)	Temp (°C)	RH (%)	O_3 (ppbv)	NO (ppbv)	NO_2 (ppbv)	CS (s^{-1})	SOA ($\mu g/m^3$)	OA ($\mu g/m^3$)
Winter	0.133	0.4	27	14.2	2.6	20.7	0.023	15.33	7.28
Spring	0.467	12.9	27	31.1	1.3	14.6	0.018	6.80	2.79
Summer	0.536	28.6	76	44.9	0.6	8.9	0.020	13.43	8.29
Autumn	0.176	12.1	65	7.2	10.0	28.3	0.023	11.14	5.01

Table S2. Mean, standard deviation (Std), median, 25 and 75 percentiles (25^{th} and 75^{th}) of total OOMs concentration in four seasons under different atmospheric conditions during daytime (08:00-16:00).

Season	Condition	Mean (cm^{-3})	Std (cm^{-3})	Median (cm^{-3})	25^{th} (cm^{-3})	75^{th} (cm^{-3})
Winter	Clean & Sunny	3.0×10^7	1.7×10^7	2.8×10^7	1.5×10^7	4.0×10^7
	Clean & Cloudy	2.1×10^7	1.1×10^7	2.0×10^7	1.1×10^7	2.6×10^7
	Polluted & Sunny	5.8×10^7	1.5×10^7	6.0×10^7	4.6×10^7	7.0×10^7
	Polluted & Cloudy	5.2×10^7	1.9×10^7	4.8×10^7	3.6×10^7	6.9×10^7
Spring	Clean & Sunny	7.9×10^7	4.1×10^7	7.5×10^7	4.5×10^7	1.0×10^8
	Clean & Cloudy	6.5×10^7	5.3×10^7	4.3×10^7	2.6×10^7	9.2×10^7
	Polluted & Sunny	2.1×10^8	4.1×10^7	2.0×10^8	1.8×10^8	2.4×10^8
	Polluted & Cloudy	1.7×10^8	1.3×10^7	1.8×10^8	1.6×10^8	1.8×10^8
Summer	Clean & Sunny	2.4×10^8	6.1×10^7	2.4×10^8	2.0×10^8	2.7×10^8
	Clean & Cloudy	1.5×10^8	6.7×10^7	1.5×10^8	9.3×10^7	2.0×10^8
	Polluted & Sunny	2.7×10^8	5.4×10^7	2.6×10^8	2.3×10^8	3.0×10^8
	Polluted & Cloudy	1.9×10^8	8.2×10^7	1.5×10^8	1.2×10^8	2.8×10^8
Autumn	Clean & Sunny	9.2×10^7	5.6×10^7	9.3×10^7	4.5×10^7	1.2×10^8
	Clean & Cloudy	9.4×10^7	3.7×10^7	9.1×10^7	6.7×10^7	1.2×10^8
	Polluted & Sunny	2.1×10^8	4.1×10^7	2.2×10^8	2.1×10^8	2.4×10^8
	Polluted & Cloudy	1.6×10^8	4.2×10^7	1.6×10^8	1.3×10^8	2.0×10^8

Table S3. Mean, standard deviation (Std), median, 25 and 75 percentiles (25^{th} and 75^{th}) of source-classified OOM concentrations in four seasons.

Season	OOMs Type	Mean (cm^{-3})	Std (cm^{-3})	Median (cm^{-3})	25th (cm^{-3})	75th (cm^{-3})
Winter	IP OOMs	2.4×10^6	1.8×10^6	1.9×10^6	9.6×10^5	3.2×10^6
	MT OOMs	1.4×10^5	8.6×10^5	1.1×10^6	7.3×10^5	1.8×10^6
	Aromatic OOMs	1.0×10^7	6.2×10^6	8.7×10^6	5.3×10^6	1.4×10^7
	Aliphatic OOMs	1.1×10^7	7.7×10^6	8.9×10^6	4.6×10^6	1.4×10^7
Spring	IP OOMs	5.2×10^6	4.5×10^6	3.8×10^6	1.9×10^6	6.8×10^6
	MT OOMs	4.2×10^6	2.6×10^6	3.5×10^6	2.3×10^6	5.3×10^6
	Aromatic OOMs	2.8×10^7	1.9×10^7	2.4×10^7	1.4×10^7	3.5×10^7
	Aliphatic OOMs	2.5×10^7	2.2×10^7	1.9×10^7	9.7×10^6	3.3×10^7
Summer	IP OOMs	5.5×10^7	3.3×10^7	5.3×10^7	2.7×10^7	7.8×10^7
	MT OOMs	8.5×10^6	2.8×10^6	8.4×10^6	6.6×10^6	1.0×10^7
	Aromatic OOMs	4.7×10^7	2.0×10^7	4.7×10^7	3.2×10^7	6.2×10^7
	Aliphatic OOMs	4.3×10^7	1.7×10^7	4.3×10^7	3.2×10^7	5.3×10^7
Autumn	IP OOMs	8.3×10^6	6.8×10^6	7.4×10^6	3.1×10^6	1.1×10^7
	MT OOMs	5.1×10^6	3.1×10^6	4.9×10^6	2.6×10^6	7.1×10^6
	Aromatic OOMs	3.0×10^7	1.7×10^7	2.8×10^7	1.7×10^7	4.1×10^7
	Aliphatic OOMs	3.4×10^7	2.3×10^7	3.2×10^7	1.5×10^7	4.9×10^7

Table S4. Nighttime OH radical and NO_3 radical concentration from previously studies in Beijing.

Measurement Site	Time Period	Radical Conc (cm^{-3})	Reference	Used Radical Conc (cm^{-3})
		OH radical		
Wangdu, Beijing, rural	2014 June	5×10^5	(Tan et al., 2017)	
Huairou, Beijing, suburban	2016 Jan.-Mar.	$2 - 4 \times 10^5$	(Tan et al., 2018)	3×10^5
Peking University, Beijing, urban	2017 Nov.-Dec.	$1 - 4 \times 10^5$	(Ma et al., 2019)	
		NO_3 radical		
Peking University, Beijing, urban	2016 May-June	$3 - 7 \times 10^8$ (calculated)	(Wang et al., 2018a)	5×10^8

Table S5. Estimated nighttime loss rate of precursor VOCs from OH radical or NO_3 radical ($Loss_{VOC\text{-}radical}$). $k_{VOC\text{-}radical}$ is the reaction rate of VOC with OH or NO_3 radical.

VOC Type	$k_{VOC\text{-}radical}$ ($cm^3\ s^{-1}$)	Reference	Used Radical Conc (cm^{-3})	$Loss_{VOC\text{-}radical}$ (s^{-1})
		OH radical		
Aromatics	$1.2 \times 10^{-12} - 5.7 \times 10^{-11}$	IUPAC MCM v3.3.1 (Atkinson and Arey, 2003)	3×10^5	$3.6 \times 10^{-7} - 1.7 \times 10^{-5}$
Aliphatics	$4.6 \times 10^{-17} - 2.4 \times 10^{-12}$			$1.4 \times 10^{-11} - 7.2 \times 10^{-7}$
Monoterpenes	$5.2 - 9.3 \times 10^{-11}$			$1.6 - 2.8 \times 10^{-5}$
Isoprene	$9.7 \times 10^{-11} – 1.2 \times 10^{-10}$			$2.9 - 3.7 \times 10^{-5}$
		NO_3 radical		
Aromatics	$< 3.0 \times 10^{-17} - 1.9 \times 10^{-15}$	IUPAC MCM v3.3.1 (Atkinson and Arey, 2003)	5×10^8	$< 1.5 \times 10^{-8} – 4.5 \times 10^{-7}$
Aliphatics	$1.1 \times 10^{-17} – 1.3 \times 10^{-16}$			$2.5 \times 10^{-9} – 6.5 \times 10^{-8}$
Monoterpenes	$2.5 - 7.7 \times 10^{-12}$			$1.3 – 3.9 \times 10^{-3}$
Isoprene	$5.3 - 7.0 \times 10^{-13}$			$2.7 – 3.5 \times 10^{-4}$

Table S6. Peak list of isoprene OOMs in this study based on the work of Xu et al. (Xu et al., 2021)

Molecular Formula	Exact Mass
CHO	
$C_4H_6O_4(NO_3^-)$	180.0150
$C_5H_8O_4(NO_3^-)$	194.0306
$C_5H_8O_5(NO_3^-)$	210.0255
$C_4H_6O_6(NO_3^-)$	212.0048
$C_5H_{10}O_5(NO_3^-)$	212.0412
$C_4H_8O_6(NO_3^-)$	214.0205
$C_5H_{12}O_5(NO_3^-)$	214.0568
$C_5H_8O_6(NO_3^-)$	226.0205
$C_5H_{10}O_6(NO_3^-)$	228.0361
$C_4H_8O_7(NO_3^-)$	230.0154
$C_5H_{12}O_6(NO_3^-)$	230.0518
$C_5H_8O_7(NO_3^-)$	242.0154
CHON	
$C_5H_9O_4N(NO_3^-)$	209.0415
$C_4H_7O_5N(NO_3^-)$	211.0208
$C_5H_9O_5N(NO_3^-)$	225.0364
$C_4H_7O_6N(NO_3^-)$	227.0157
$C_5H_9O_6N(NO_3^-)$	241.0314
$C_4H_7O_7N(NO_3^-)$	243.0106
$C_5H_{11}O_6N(NO_3^-)$	243.0470
$C_5H_9O_7N(NO_3^-)$	257.0263
$C_5H_{11}O_7N(NO_3^-)$	259.0419
$C_5H_9O_8N(NO_3^-)$	273.0212
$C_4H_7O_9N(NO_3^-)$	275.0004
$C_5H_{11}O_8N(NO_3^-)$	275.0368
$C_5H_{11}O_9N(NO_3^-)$	291.0317
$C_5H_9O_{10}N(NO_3^-)$	305.0110
$CHON_{2,3}$	
$C_5H_{10}O_6N_2(NO_3\text{-})$	256.0423
$C_4H_8O_7N_2\ (NO_3\text{-})$	258.0215
$C_5H_{10}O_7N_2(NO_3\text{-})$	272.0372
$C_5H_{10}O_8N_2(NO_3\text{-})$	288.0321
$C_5H_{10}O_9N_2(NO_3\text{-})$	304.0270

$C_4H_8O_{10}N_2(NO_3\text{-})$	306.0063
$C_5H_{10}O_{10}N_2\ (NO_3\text{-})$	320.0219
$C_5H_9O_{10}N_3(NO_3\text{-})$	333.0172

Table S7 Fractions of typical IP OOM molecules in total IP OOMs.

Formula	Winter	Spring	Summer	Autumn
		CHO		
C4H8O7	4.58%	0.63%	0.07%	0.53%
C5H8O4	13.80%	12.42%	2.69%	16.76%
C5H8O5	4.70%	6.03%	0.94%	2.74%
C5H8O6	7.90%	5.03%	0.29%	1.54%
C5H10O5	0.22%	0.33%	0.20%	0.20%
C5H10O6	0.38%	0.79%	0.22%	0.93%
C5H12O6	0.85%	0.58%	0.03%	0.45%
		CHON		
C4H7O5N	7.16%	6.27%	1.95%	12.95%
C4H7O6N	10.75%	13.68%	5.70%	7.64%
C4H7O7N	1.95%	1.54%	0.58%	1.02%
C5H9O4N	0.57%	0.51%	0.53%	0.85%
C5H9O5N	7.10%	4.43%	1.20%	7.86%
C5H9O6N	10.76%	18.24%	4.90%	13.04%
C5H9O7N	1.78%	2.57%	3.33%	2.07%
C5H11O6N	2.24%	2.59%	6.40%	2.54%
C5H11O7N	0.64%	0.52%	0.26%	0.26%
C5H11O8N	0.65%	0.41%	0.13%	0.29%
		$CHON_2$		
C4H8O7N2	1.23%	3.11%	0.08%	3.10%
C5H10O7N2	8.02%	5.75%	0.50%	7.46%
C5H10O8N2	8.41%	10.26%	58.21%	13.06%
C5H10O9N2	NaN	NaN	0.89%	0.57%
		$CHON_3$		
C5H9O10N3	2.42%	1.76%	9.26%	2.34%

Table S8 Fractions of typical MT OOM molecules in total MT OOMs.

Formula	Winter	Spring	Summer	Autumn
		CHO		
C10H14O4	2.3%	1.2%	1.4%	1.8%
C10H14O5	2.7%	2.2%	2.3%	1.9%
C10H14O6	NaN	1.0%	2.9%	1.5%
C10H14O7	1.2%	1.3%	0.9%	0.5%
C10H16O4	2.3%	1.5%	1.7%	2.8%
C10H16O5	2.7%	1.3%	2.8%	2.6%
C10H16O6	1.5%	1.5%	2.2%	1.4%
C10H18O4	2.2%	1.5%	1.2%	2.1%
C10H18O5	0.6%	0.6%	0.9%	0.8%
		CHON		
C10H13O6N	1.4%	1.0%	0.6%	1.3%
C10H13O7N	1.8%	1.7%	1.6%	1.6%
C10H13O8N	1.0%	1.1%	1.0%	0.9%
C10H13O9N	0.6%	0.7%	0.8%	0.4%
C10H15O6N	10.7%	7.7%	8.4%	12.5%
C10H15O7N	9.9%	10.6%	8.6%	9.3%
C10H15O8N	7.3%	9.6%	8.7%	5.5%
C10H15O9N	2.5%	NaN	2.5%	1.3%
C10H17O6N	8.4%	5.6%	7.0%	11.2%
C10H17O7N	5.2%	7.7%	8.1%	10.2%
C10H17O8N	2.6%	4.3%	4.7%	2.0%

C10H17O9N	0.4%	1.4%	1.5%	0.8%
		$CHON_2$		
C10H12O8N2	0.7%	0.4%	NaN	0.3%
C10H12O9N2	0.7%	0.4%	0.3%	0.3%
C10H12O10N2	0.3%	0.2%	NaN	0.2%
C10H14O8N2	0.7%	0.8%	0.9%	0.8%
C10H14O9N2	2.3%	1.1%	1.2%	1.4%
C10H14O10N2	0.9%	1.0%	1.2%	0.9%
C10H16O8N2	3.5%	8.7%	6.3%	9.7%
C10H16O9N2	4.3%	7.0%	6.9%	3.1%
C10H16O10N2	3.1%	5.7%	5.2%	3.4%

Table S9 Fractions of typical aromatic OOM molecules in total aromatic OOMs.

Formula	Winter	Spring	Summer	Autumn	(Garmash et al., 2020)	(Molteni et al., 2018)
			CHO			
C5H4O5	0.10%	0.29%	0.17%	0.18%	×	×
C5H4O6	0.17%	0.16%	NaN	NaN	√	×
C5H6O5	0.90%	1.16%	0.72%	0.68%	×	√
C5H7O6	0.73%	0.44%	0.38%	0.17%	×	×
C6H6O4	NaN	0.76%	0.43%	0.80%	√	√
C6H6O5	0.90%	0.81%	0.26%	0.37%	√	√
C6H8O4	1.96%	1.41%	1.32%	2.18%	√	√
C6H8O5	1.29%	1.41%	0.93%	0.94%	√	√
C6H8O6	NaN	0.41%	0.31%	0.27%	√	√
C6H8O7	0.54%	0.24%	0.26%	0.11%	√	√
C7H8O4	0.98%	0.54%	0.64%	0.90%	√	√
C7H8O5	1.52%	1.33%	1.74%	0.96%	√	√
C7H8O6	0.33%	0.24%	0.12%	0.10%	√	√
C7H10O3	0.16%	0.09%	0.12%	0.38%	√	×
C7H10O4	1.47%	1.43%	2.06%	2.24%	√	√
C7H10O5	1.12%	1.48%	1.37%	1.11%	√	√
C7H10O6	0.18%	0.29%	0.66%	0.44%	√	√
C7H10O7	0.11%	0.08%	0.18%	0.27%	√	√
C7H10O8	0.08%	0.08%	0.08%	0.07%	√	√
C7H12O6	0.26%	0.20%	0.16%	0.05%	√	√
C7H12O7	0.12%	0.12%	NaN	0.07%	√	√
C8H10O3	0.30%	0.10%	NaN	0.16%		×
C8H10O4	0.72%	0.42%	0.51%	0.77%		√
C8H10O5	1.41%	1.37%	1.54%	1.35%		√
C8H12O3	0.24%	0.08%	0.08%	0.27%		×
C8H12O4	1.51%	1.91%	2.17%	2.77%		√
C8H12O5	0.97%	0.94%	1.92%	0.93%	no xylene experiment	√
C8H12O6	0.73%	0.66%	0.71%	0.56%		√
C8H12O7	NaN	0.19%	0.22%	0.11%		√
C8H12O8	NaN	0.15%	0.17%	0.15%		√
C8H14O6	NaN	0.13%	0.23%	0.01%		√
C8H14O7	NaN	0.07%	0.10%	0.11%		√
C9H12O4	NaN	0.18%	0.45%	0.51%		×
C9H12O5	0.72%	0.51%	0.70%	0.44%		×
C9H12O6	NaN	0.19%	0.43%	0.45%		√
C9H12O7	0.24%	0.15%	0.67%	0.08%	no C9 aromatic hydrocarbon experiment	×
C9H14O3	1.23%	0.28%	0.19%	0.55%		×
C9H14O4	0.85%	0.61%	0.67%	1.02%		×
C9H14O5	0.64%	0.87%	0.92%	0.77%		√
C9H14O6	0.46%	0.33%	0.65%	0.34%		√
C9H14O7	NaN	NaN	0.26%	0.11%		√

C9H16O6	NaN	0.09%	0.20%	0.10%		×
C9H16O7	NaN	0.08%	0.10%	0.12%		√
C10H14O2	NaN	0.01%	0.02%	0.02%	×	no C10 aromatic hydrocarbon experiment
C10H14O3	0.16%	0.05%	0.03%	0.11%	×	
			CHON			
C5H5O4N	0.41%	0.28%	0.19%	0.34%	√	
C5H5O5N	0.32%	0.20%	0.09%	0.19%	√	
C5H5O7N	0.48%	0.43%	0.29%	0.11%	×	
C5H7O8N	NaN	NaN	0.75%	0.21%	√	
C6H5O6N	0.38%	0.22%	0.09%	0.14%	√	
C6H7O3N	1.00%	0.42%	NaN	0.06%	×	
C6H7O4N	0.69%	0.48%	0.31%	0.73%	×	
C6H7O5N	0.66%	0.31%	0.13%	0.39%	√	
C6H7O6N	1.71%	1.10%	0.47%	0.90%	×	
C6H7O7N	0.23%	0.19%	0.58%	0.35%	√	
C6H7O8N	0.28%	0.18%	NaN	NaN	√	
C6H9O8N	0.38%	0.27%	0.44%	0.24%	×	
C6H9O9N	NaN	NaN	0.19%	NaN	√	
C7H7O5N	0.25%	0.14%	0.14%	0.27%		
C7H7O6N	0.47%	0.15%	0.28%	0.29%		
C7H7O7N	0.26%	0.14%	NaN	NaN		
C7H7O8N	0.17%	0.17%	0.13%	0.07%		
C7H7O9N	0.15%	0.14%	0.17%	0.06%		
C7H9O5N	0.77%	0.35%	0.21%	0.49%		
C7H9O6N	2.31%	1.93%	1.25%	1.97%	no toluene + NO_x experiment	
C7H9O7N	1.13%	1.38%	1.83%	0.92%		
C7H9O8N	0.34%	1.01%	1.12%	0.27%		
C7H9O9N	0.09%	NaN	0.15%	0.05%		
C7H9O10N	NaN	NaN	0.17%	0.06%		
C7H11O8N	0.50%	0.49%	0.71%	0.27%		
C7H11O9N	0.16%	0.21%	0.22%	0.18%		
C8H9O5N	0.28%	0.26%	0.27%	0.36%		no NO_x experiment
C8H9O6N	0.30%	0.22%	0.20%	0.25%		
C8H9O7N	0.34%	0.38%	0.22%	0.14%		
C8H9O8N	0.09%	0.20%	0.09%	0.04%		
C8H9O9N	0.18%	0.15%	0.16%	0.08%		
C8H11O5N	0.41%	0.18%	0.14%	0.27%		
C8H11O6N	3.88%	2.03%	0.71%	3.38%		
C8H11O7N	1.30%	1.61%	2.87%	1.50%	no xylene experiment	
C8H11O8N	1.11%	1.58%	1.53%	0.77%		
C8H11O9N	0.25%	0.34%	0.21%	0.14%		
C8H11O10N	0.20%	0.16%	0.13%	NaN		
C8H13O8N	0.58%	0.65%	0.89%	0.51%		
C8H13O9N	NaN	NaN	0.37%	0.10%		
C8H13O10N	0.07%	0.10%	0.17%	0.06%		
C9H11O5N	0.13%	0.14%	0.11%	0.14%		
C9H11O6N	0.31%	0.23%	0.17%	0.19%		
C9H11O7N	0.35%	0.38%	0.27%	0.15%		
C9H11O8N	0.16%	0.24%	0.20%	0.08%		
C9H11O9N	0.14%	0.19%	NaN	0.12%		
C9H11O10N	0.06%	0.32%	0.13%	0.04%	no C9 aromatic hydrocarbon experiment	
C9H13O5N	0.29%	0.13%	0.15%	0.24%		
C9H13O6N	2.71%	1.20%	0.69%	2.22%		
C9H13O7N	1.40%	1.15%	1.86%	1.28%		
C9H13O8N	1.56%	1.67%	1.61%	0.99%		
C9H13O9N	0.43%	0.49%	0.40%	0.18%		
C9H13O10N	0.12%	0.19%	0.18%	0.12%		

C9H15O8N	0.51%	0.72%	1.27%	0.51%		
C9H15O9N	0.14%	0.23%	0.36%	0.15%		
C9H15O10N	NaN	0.20%	0.18%	NaN		
				$CHON_2$		
C8H10O8N2	0.11%	0.11%	0.05%	0.10%		
C8H10O9N2	NaN	NaN	0.19%	NaN		
C8H10O10N2	0.24%	0.18%	0.23%	0.16%		
C8H10O11N2	0.07%	0.07%	0.10%	0.03%	no xylene experiment	
C8H12O10N2	0.22%	0.48%	1.01%	0.48%		
C8H12O11N2	0.04%	NaN	0.15%	0.07%		
C8H12O12N2	0.08%	0.04%	0.05%	0.03%		no NO_x experiment
C9H12O8N2	0.14%	0.14%	0.15%	0.05%		
C9H12O9N2	NaN	0.48%	0.25%	0.16%		
C9H12O10N2	0.22%	0.24%	0.26%	0.14%	no C9 aromatic hydrocarbon experiment	
C9H12O11N2	0.06%	NaN	0.12%	0.04%		
C9H14O10N2	0.27%	0.58%	0.90%	0.47%		
C9H14O11N2	0.03%	0.10%	0.16%	0.10%		
Sum	54.99%	50.31%	53.93%	48.51%	——	——

Table S10 Fractions of DBE≤4 and DBE>4 compounds for nC≤9 and nC≥10 aromatic OOMs in four seasons.

OOM Type	Winter	Spring	Summer	Autumn
nC≤9 aromatic OOMs				
DBE≤4	83%	80%	83%	84%
DBE>4	17%	20%	17%	16%
nC≥10 aromatic OOMs				
DBE≤4	34%	32%	41%	33%
DBE>4	66%	68%	59%	67%

Table S11 Fractions of typical aliphatic OOM molecules in total aliphatic OOMs.

Formula	Winter	Spring	Summer	Autumn
CHO				
C6H10O4	1.68%	1.82%	1.55%	2.31%
C7H12O4	1.05%	1.23%	1.16%	1.58%
C8H14O4	0.50%	0.73%	0.55%	0.92%
C9H16O4	0.41%	0.67%	0.51%	1.04%
CHON				
C5H7O6N	7.60%	7.50%	7.52%	4.67%
C6H9O6N	8.65%	6.40%	3.63%	6.82%
C6H11O5N	1.86%	0.84%	0.97%	2.39%
C6H11O6N	2.56%	4.59%	6.96%	5.44%
C7H11O5N	1.08%	0.52%	0.34%	0.96%
C7H11O6N	5.69%	5.05%	3.53%	3.92%
C7H13O5N	1.06%	0.50%	0.51%	1.37%
C7H13O6N	1.46%	2.09%	2.37%	1.38%
C7H13O7N	0.30%	0.46%	0.47%	0.30%
C8H13O6N	3.06%	2.41%	2.01%	2.72%
C8H15O5N	0.87%	0.27%	0.40%	0.83%
C8H15O6N	1.15%	1.58%	1.68%	1.13%
C8H15O7N	0.27%	0.52%	0.68%	0.25%
C8H17O5N	0.59%	0.25%	0.17%	0.75%
C9H15O5N	1.01%	0.25%	0.17%	0.38%
C9H15O6N	1.51%	2.66%	2.76%	2.79%
C9H17O5N	0.67%	0.29%	0.36%	0.94%
C9H17O6N	0.86%	1.46%	2.21%	1.35%
C9H17O7N	0.20%	0.92%	0.47%	0.36%
C10H17O5N	0.44%	0.19%	0.18%	0.74%
C10H17O6N	1.05%	1.08%	1.28%	1.71%

C10H19O5N	0.54%	0.22%	0.25%	0.74%
C10H19O6N	0.48%	1.14%	1.04%	0.86%
C11H19O6N	0.27%	0.32%	0.42%	0.51%
$CHON_2$				
C4H8O8N2	1.07%	NaN	0.88%	0.54%
C5H8O8N2	1.04%	NaN	4.80%	0.77%
C6H10O8N2	1.38%	1.89%	2.37%	1.38%
C6H10O9N2	0.77%	0.83%	0.81%	0.57%
C6H12O7N2	4.07%	2.54%	NaN	2.43%
C7H12O8N2	1.39%	1.55%	1.58%	1.15%
C7H12O9N2	0.37%	0.59%	0.45%	0.41%
C7H14O7N2	3.31%	1.71%	0.39%	1.98%
C7H14O8N2	0.38%	0.36%	0.35%	0.39%
C8H14O8N2	1.64%	2.43%	1.82%	1.10%
C8H16O7N2	2.60%	1.38%	0.37%	1.91%
C8H16O8N2	0.25%	0.59%	0.35%	0.32%
C9H16O8N2	1.14%	1.40%	1.28%	1.03%
C9H18O7N2	1.85%	0.65%	0.22%	1.07%
C10H18O8N2	0.76%	1.67%	1.95%	1.20%
C10H20O7N2	0.97%	0.41%	NaN	0.55%
C11H22O7N2	0.59%	0.27%	0.19%	0.69%
C12H24O7N2	0.32%	0.32%	0.14%	0.47%
C13H26O7N2	0.14%	0.20%	0.12%	0.26%
C14H28O7N2	0.07%	0.13%	0.10%	0.16%
$C_nH_{2n}O_7N_2$ (n=6-14)	14.15%	7.75%	1.68%	9.74%

Table S12. The median volatility ($\log_{10}$ [C^* (μg·cm$_{-3}$)]) of $C_{6\text{-}14}H_{12\text{-}28}O_7N_2$ compounds during the winter period (5th January to 14th February, 2019).

Compound	$\log_{10}$ [C^*(μg·cm^{-3})]	Volatility Type
$C_6H_{12}O_7N_2$	1.47	semi-volatile organic compounds
$C_7H_{14}O_7N_2$	1.02	
$C_8H_{16}O_7N_2$	0.55	
$C_9H_{18}O_7N_2$	0.07	
$C_{10}H_{20}O_7N_2$	-0.41	
$C_{11}H_{22}O_7N_2$	-0.90	low-volatility organic compounds
$C_{12}H_{24}O_7N_2$	-1.39	
$C_{13}H_{26}O_7N_2$	-1.88	
$C_{14}H_{28}O_7N_2$	-2.38	

Table S13. Concentrations of aromatic and aliphatic OOMs in Beijing and other Chinese megacities.

Measurement Site	Time Period	Aromatic OOMs (cm^{-3})	Aliphatic OOMs (cm^{-3})	Reference
Beijing, China	2019 Jan.-Feb.	1.0×10^7	1.1×10^7	This study
	2019 Mar.-Apr.	2.8×10^7	2.5×10^7	
	2019 July-Aug.	4.7×10^7	4.3×10^7	
	2019 Oct.-Nov.	3.0×10^7	3.4×10^7	
Hong Kong, China	2018 Nov.	8.1×10^7	9.7×10^7	2022, Nie et al.
Shanghai, China	2018 Nov.	3.2×10^7	3.0×10^7	2022, Nie et al.
Nanjing, China	2018 Nov.	2.5×10^7	3.7×10^7	2022, Nie et al.

Table S14. Common aromatic and aliphatic OOM molecules in this study and reported in Liu et al. (Liu et al., 2021).

Aromatic OOMs	Aliphatic OOMs
$C_{6\text{-}8}H_{8\text{-}12}O_4$	
$C_8H_{11}O_{6\text{-}8}N$	$C_{5\text{-}7}H_{7\text{-}11}O_6N$
$C_9H_{17}O_{7,8}N$	$C_6H_{11}O_6N$
$C_{10}H_{15}O_8N$	

$C_8H_{12}O_{10}N_2$	$C_{6\text{-}10}H_{10\text{-}18}O_8N_2$

Table S15. Median concentrations of ELVOCs, LVOCs and SVOCs of total OOMs in four seasons.

Season	ELVOCs (cm^{-3})	LVOCs (cm^{-3})	SVOCs (cm^{-3})
Winter	1.4×10^6	9.4×10^6	5.3×10^6
Spring	8.6×10^6	2.0×10^7	1.5×10^7
Summer	1.3×10^7	4.0×10^7	8.4×10^7
Autumn	9.6×10^6	2.8×10^7	2.9×10^7

Table S16. Volatility distribution of source-classified OOMs in four seasons.

Season	OOMs Type	ELVOCs + LVOCs	SVOCs	IVOCs + VOCs
Winter	IP OOMs	42.1 %	56.3 %	1.6 %
	MT OOMs	100.0 %	0.0 %	0.0 %
	Aromatic OOMs	77.5 %	13.4 %	9.1 %
	Aliphatic OOMs	54.7 %	38.2 %	7.1 %
Spring	IP OOMs	25.2 %	56.2 %	18.5 %
	MT OOMs	95.7 %	4.3 %	0.0 %
	Aromatic OOMs	69.3 %	21.2 %	9.6 %
	Aliphatic OOMs	38.2 %	50.5 %	11.3 %
Summer	IP OOMs	3.3 %	92.2 %	4.5 %
	MT OOMs	70.9 %	29.1 %	0.0 %
	Aromatic OOMs	73.8 %	20.8 %	5.4 %
	Aliphatic OOMs	17.8 %	71.5 %	10.7 %
Autumn	IP OOMs	15.8 %	48.1 %	36.1 %
	MT OOMs	93.6 %	6.4 %	0.0 %
	Aromatic OOMs	66.7 %	21.6 %	11.7 %
	Aliphatic OOMs	30.0 %	62.0 %	8.0 %

Table S17 Concentrations of NO, *n*-decane, cyclohexane and decalin as well as corresponding VOC to NO ratios in the Leipzig free-jet flow reactor experiments of Wang et al. (Wang et al., 2021)

NO (ppb)	0.17	1.15	2.27	3.42	4.46	7.0	8.93
n-decane (ppb)				130			
n-decane / NO	745	113	57	38	29	19	15
cyclohexane (ppb)				558			
cyclohexane / NO	3192	484	246	163	125	83	63
decalin (ppb)				74			
decalin / NO	426	65	33	22	17	11	8

Table S18. NO_x, total hydrocarbons (HCs) and hydrocarbon to NO_x ratios (HCs / NO_x) for urban Beijing. The NO_x concentration are the measured ones (mean values) in this study. Hydrocarbon concentrations are taken from literatures (Zhang et al., 2017;Zhang et al., 2020).

	Winter	Spring	Summer	Autumn
NO (ppb)	15.7	6.7	1.6	24.7
NO_2 (ppb)	23.8	18.6	10.9	27.1
NO_x (ppb)	39.9	25.2	12.0	51.6
2017, Hao Zhang et al.				
Total HCs (ppb)	47.72	25.63	20.09	39.25
HCs / NO_x	1.20	1.02	1.67	0.76
2020, Lihui Zhang et al.				
Total HCs (ppb)	16.37	9.0	11.61	12.95
HCs / NO_x	0.41	0.36	0.97	0.25

To c

REFERENCES

Atkinson, R., and Arey, J.: Atmospheric Degradation of Volatile Organic Compounds, Chemical Reviews, 103, 4605-4638, 10.1021/cr0206420, 2003.

Berndt, T., Richters, S., Jokinen, T., Hyttinen, N., Kurtén, T., Otkjær, R. V., Kjaergaard, H. G., Stratmann, F., Herrmann, H., Sipilä, M., Kulmala, M., and Ehn, M.: Hydroxyl radical-induced formation of highly oxidized organic compounds, Nature Communications, 7, 13677, 10.1038/ncomms13677, 2016.

Bianchi, F., Kurten, T., Riva, M., Mohr, C., Rissanen, M. P., Roldin, P., Berndt, T., Crounse, J. D., Wennberg, P. O., Mentel, T. F., Wildt, J., Junninen, H., Jokinen, T., Kulmala, M., Worsnop, D. R., Thornton, J. A., Donahue, N., Kjaergaard, H. G., and Ehn, M.: Highly Oxygenated Organic Molecules (HOM) from Gas-Phase Autoxidation Involving Peroxy Radicals: A Key Contributor to Atmospheric Aerosol, Chemical Reviews, 119, 3472-3509, 10.1021/acs.chemrev.8b00395, 2019.

D'Ambro, E. L., Møller, K. H., Lopez-Hilfiker, F. D., Schobesberger, S., Liu, J., Shilling, J. E., Lee, B. H., Kjaergaard, H. G., and Thornton, J. A.: Isomerization of Second-Generation Isoprene Peroxy Radicals: Epoxide Formation and Implications for Secondary Organic Aerosol Yields, Environmental Science & Technology, 51, 4978-4987, 10.1021/acs.est.7b00460, 2017.

Dada, L., Paasonen, P., Nieminen, T., Buenrostro Mazon, S., Kontkanen, J., Peräkylä, O., Lehtipalo, K., Hussein, T., Petäjä, T., Kerminen, V. M., Bäck, J., and Kulmala, M.: Long-term analysis of clear-sky new particle formation events and nonevents in Hyytiälä, Atmos. Chem. Phys., 17, 6227-6241, 10.5194/acp-17-6227-2017, 2017.

Donahue, N. M., Robinson, A. L., Stanier, C. O., and Pandis, S. N.: Coupled Partitioning, Dilution, and Chemical Aging of Semivolatile Organics, Environmental Science & Technology, 40, 2635-2643, 10.1021/es052297c, 2006.

Donahue, N. M., Epstein, S. A., Pandis, S. N., and Robinson, A. L.: A two-dimensional volatility basis set: 1. organic-aerosol mixing thermodynamics, Atmos. Chem. Phys., 11, 3303-3318, 10.5194/acp-11-3303-2011, 2011.

Donahue, N. M., Kroll, J. H., Pandis, S. N., and Robinson, A. L.: A two-dimensional volatility basis set – Part 2: Diagnostics of organic-aerosol evolution, Atmos. Chem. Phys., 12, 615-634, 10.5194/acp-12-615-2012, 2012.

Ehn, M., Thornton, J. A., Kleist, E., Sipilä, M., Junninen, H., Pullinen, I., Springer, M., Rubach, F., Tillmann, R., Lee, B., Lopez-Hilfiker, F., Andres, S., Acir, I.-H., Rissanen, M., Jokinen, T., Schobesberger, S., Kangasluoma, J., Kontkanen, J., Nieminen, T., Kurtén, T., Nielsen, L. B., Jørgensen, S., Kjaergaard, H. G., Canagaratna, M., Maso, M. D., Berndt, T., Petäjä, T., Wahner, A., Kerminen, V.-M., Kulmala, M., Worsnop, D. R., Wildt, J., and Mentel, T. F.: A large source of low-volatility secondary organic aerosol, Nature, 506, 476-479, 10.1038/nature13032, 2014.

Epstein, S. A., Riipinen, I., and Donahue, N. M.: A Semiempirical Correlation between Enthalpy of Vaporization and Saturation Concentration for Organic Aerosol, Environmental Science & Technology, 44, 743-748, 10.1021/es902497z, 2010.

Garmash, O., Rissanen, M. P., Pullinen, I., Schmitt, S., Kausiala, O., Tillmann, R., Zhao, D., Percival, C., Bannan, T. J., Priestley, M., Hallquist, A. M., Kleist, E., Kiendler-Scharr, A., Hallquist, M., Berndt, T., McFiggans, G., Wildt, J., Mentel, T., and Ehn, M.: Multi-generation OH oxidation as a source for highly oxygenated organic molecules from aromatics, Atmospheric Chemistry and Physics, 20, 515-537, 10.5194/acp-20-515-2020, 2020.

Hyttinen, N., Kupiainen-Määttä, O., Rissanen, M. P., Muuronen, M., Ehn, M., and Kurtén, T.: Modeling the Charging of Highly Oxidized Cyclohexene Ozonolysis Products Using Nitrate-Based Chemical Ionization, The Journal of Physical Chemistry A, 119, 6339-6345, 10.1021/acs.jpca.5b01818, 2015.

Jokinen, T., Sipilä, M., Richters, S., Kerminen, V.-M., Paasonen, P., Stratmann, F., Worsnop, D., Kulmala, M., Ehn, M., Herrmann, H., and Berndt, T.: Rapid Autoxidation Forms Highly Oxidized RO_2 Radicals in the Atmosphere, Angewandte Chemie International Edition, 53, 14596-14600, https://doi.org/10.1002/anie.201408566, 2014.

Lee, L., Teng, A. P., Wennberg, P. O., Crounse, J. D., and Cohen, R. C.: On Rates and Mechanisms of OH and O_3 Reactions with Isoprene-Derived Hydroxy Nitrates, The Journal of Physical Chemistry A, 118, 1622-1637, 10.1021/jp4107603, 2014.

Liu, Y., Nie, W., Li, Y., Ge, D., Liu, C., Xu, Z., Chen, L., Wang, T., Wang, L., Sun, P., Qi, X., Wang, J., Xu, Z., Yuan, J., Yan, C., Zhang, Y., Huang, D., Wang, Z., Donahue, N. M., Worsnop, D., Chi, X., Ehn, M., and Ding, A.: Formation of condensable organic vapors from anthropogenic and biogenic volatile organic compounds (VOCs) is strongly perturbed by NO_x in eastern China, Atmos. Chem. Phys., 21, 14789-14814, 10.5194/acp-21-14789-2021, 2021.

Ma, X., Tan, Z., Lu, K., Yang, X., Liu, Y., Li, S., Li, X., Chen, S., Novelli, A., Cho, C., Zeng, L., Wahner, A., and Zhang, Y.: Winter photochemistry in Beijing: Observation and model simulation of OH and HO_2 radicals at an urban site, Science of The Total Environment, 685, 85-95, https://doi.org/10.1016/j.scitotenv.2019.05.329, 2019.

Massoli, P., Stark, H., Canagaratna, M. R., Krechmer, J. E., Xu, L., Ng, N. L., Mauldin, R. L., Yan, C., Kimmel, J., Misztal, P. K., Jimenez, J. L., Jayne, J. T., and Worsnop, D. R.: Ambient Measurements of Highly Oxidized Gas-Phase Molecules during the Southern Oxidant and Aerosol Study (SOAS) 2013, ACS Earth and Space Chemistry, 2, 653-672, 10.1021/acsearthspacechem.8b00028, 2018.

Mohr, C., Thornton, J. A., Heitto, A., Lopez-Hilfiker, F. D., Lutz, A., Riipinen, I., Hong, J., Donahue, N. M., Hallquist, M., Petaja, T., Kulmala, M., and Yli-Juuti, T.: Molecular identification of organic vapors driving atmospheric nanoparticle growth, Nature Communications, 10, 10.1038/s41467-019-12473-2, 2019.

Molteni, U., Bianchi, F., Klein, F., El Haddad, I., Frege, C., Rossi, M. J., Dommen, J., and Baltensperger, U.: Formation of highly oxygenated organic molecules from aromatic compounds, Atmos. Chem. Phys., 18, 1909-1921, 10.5194/acp-18-1909-2018, 2018.

Praplan, A. P., Schobesberger, S., Bianchi, F., Rissanen, M. P., Ehn, M., Jokinen, T., Junninen, H., Adamov, A., Amorim, A., Dommen, J., Duplissy, J., Hakala, J., Hansel, A., Heinritzi, M., Kangasluoma, J., Kirkby, J., Krapf, M., Kürten, A., Lehtipalo, K., Riccobono, F., Rondo, L., Sarnela, N., Simon, M., Tomé, A., Tröstl, J., Winkler, P. M., Williamson, C., Ye, P., Curtius, J., Baltensperger, U., Donahue, N. M., Kulmala, M., and Worsnop, D. R.: Elemental composition and clustering behaviour of α-pinene oxidation products for different oxidation conditions, Atmos. Chem. Phys., 15, 4145-4159, 10.5194/acp-15-4145-2015, 2015.

Rissanen, M. P., Kurtén, T., Sipilä, M., Thornton, J. A., Kangasluoma, J., Sarnela, N., Junninen, H., Jørgensen, S., Schallhart, S., Kajos, M. K., Taipale, R., Springer, M., Mentel, T. F., Ruuskanen, T., Petäjä, T., Worsnop, D. R., Kjaergaard, H. G., and Ehn, M.: The Formation of Highly Oxidized Multifunctional Products in the Ozonolysis of Cyclohexene, Journal of the American Chemical Society, 136, 15596-15606, 10.1021/ja507146s, 2014.

Rissanen, M. P.: NO2 Suppression of Autoxidation–Inhibition of Gas-Phase Highly Oxidized Dimer Product Formation, ACS Earth and Space Chemistry, 2, 1211-1219, 10.1021/acsearthspacechem.8b00123, 2018.

Schwantes, R. H., Teng, A. P., Nguyen, T. B., Coggon, M. M., Crounse, J. D., St. Clair, J. M., Zhang, X., Schilling, K. A., Seinfeld, J. H., and Wennberg, P. O.: Isoprene NO3 Oxidation Products from the RO_2 + HO_2 Pathway, The Journal of Physical Chemistry A, 119, 10158-10171, 10.1021/acs.jpca.5b06355, 2015.

Seinfeld, J. H., and Pandis, S. N.: Atmospheric chemistry and physics: from air pollution to climate change, John Wiley & Sons, 2016.

Stolzenburg, D., Fischer, L., Vogel, A. L., Heinritzi, M., Schervish, M., Simon, M., Wagner, A. C., Dada, L., Ahonen, L. R., Amorim, A., Baccarini, A., Bauer, P. S., Baumgartner, B., Bergen, A., Bianchi, F., Breitenlechner, M., Brilke, S., Buenrostro Mazon, S., Chen, D., Dias, A., Draper, D. C., Duplissy, J., El Haddad, I., Finkenzeller, H., Frege, C., Fuchs, C., Garmash, O., Gordon, H., He, X., Helm, J., Hofbauer, V., Hoyle, C. R., Kim, C., Kirkby, J., Kontkanen, J., Kürten, A., Lampilahti, J., Lawler, M., Lehtipalo, K., Leiminger, M., Mai, H., Mathot, S., Mentler, B., Molteni, U., Nie, W., Nieminen, T., Nowak, J. B., Ojdanic, A., Onnela, A., Passananti, M., Petäjä, T., Quéléver, L. L. J., Rissanen, M. P., Sarnela, N., Schallhart, S., Tauber, C., Tomé, A., Wagner, R., Wang, M., Weitz, L., Wimmer, D., Xiao, M., Yan, C., Ye, P., Zha, Q., Baltensperger, U., Curtius, J., Dommen, J., Flagan, R. C., Kulmala, M., Smith, J. N., Worsnop, D. R., Hansel,

A., Donahue, N. M., and Winkler, P. M.: Rapid growth of organic aerosol nanoparticles over a wide tropospheric temperature range, Proceedings of the National Academy of Sciences, 115, 9122, 10.1073/pnas.1807604115, 2018.
Tan, Z., Fuchs, H., Lu, K., Hofzumahaus, A., Bohn, B., Broch, S., Dong, H., Gomm, S., Häseler, R., He, L., Holland, F., Li, X., Liu, Y., Lu, S., Rohrer, F., Shao, M., Wang, B., Wang, M., Wu, Y., Zeng, L., Zhang, Y., Wahner, A., and Zhang, Y.: Radical chemistry at a rural site (Wangdu) in the North China Plain: observation and model calculations of OH, HO_2 and RO_2 radicals, Atmos. Chem. Phys., 17, 663-690, 10.5194/acp-17-663-2017, 2017.
Tan, Z., Rohrer, F., Lu, K., Ma, X., Bohn, B., Broch, S., Dong, H., Fuchs, H., Gkatzelis, G. I., Hofzumahaus, A., Holland, F., Li, X., Liu, Y., Liu, Y., Novelli, A., Shao, M., Wang, H., Wu, Y., Zeng, L., Hu, M., Kiendler-Scharr, A., Wahner, A., and Zhang, Y.: Wintertime photochemistry in Beijing: observations of ROx radical concentrations in the North China Plain during the BEST-ONE campaign, Atmos. Chem. Phys., 18, 12391-12411, 10.5194/acp-18-12391-2018, 2018.
Teng, A. P., Crounse, J. D., and Wennberg, P. O.: Isoprene Peroxy Radical Dynamics, Journal of the American Chemical Society, 139, 5367-5377, 10.1021/jacs.6b12838, 2017.
Tröstl, J., Chuang, W. K., Gordon, H., Heinritzi, M., Yan, C., Molteni, U., Ahlm, L., Frege, C., Bianchi, F., Wagner, R., Simon, M., Lehtipalo, K., Williamson, C., Craven, J. S., Duplissy, J., Adamov, A., Almeida, J., Bernhammer, A.-K., Breitenlechner, M., Brilke, S., Dias, A., Ehrhart, S., Flagan, R. C., Franchin, A., Fuchs, C., Guida, R., Gysel, M., Hansel, A., Hoyle, C. R., Jokinen, T., Junninen, H., Kangasluoma, J., Keskinen, H., Kim, J., Krapf, M., Kürten, A., Laaksonen, A., Lawler, M., Leiminger, M., Mathot, S., Möhler, O., Nieminen, T., Onnela, A., Petäjä, T., Piel, F. M., Miettinen, P., Rissanen, M. P., Rondo, L., Sarnela, N., Schobesberger, S., Sengupta, K., Sipilä, M., Smith, J. N., Steiner, G., Tomè, A., Virtanen, A., Wagner, A. C., Weingartner, E., Wimmer, D., Winkler, P. M., Ye, P., Carslaw, K. S., Curtius, J., Dommen, J., Kirkby, J., Kulmala, M., Riipinen, I., Worsnop, D. R., Donahue, N. M., and Baltensperger, U.: The role of low-volatility organic compounds in initial particle growth in the atmosphere, Nature, 533, 527-531, 10.1038/nature18271, 2016.
Wang, H., Lu, K., Guo, S., Wu, Z., Shang, D., Tan, Z., Wang, Y., Le Breton, M., Lou, S., Tang, M., Wu, Y., Zhu, W., Zheng, J., Zeng, L., Hallquist, M., Hu, M., and Zhang, Y.: Efficient N_2O_5 uptake and NO_3 oxidation in the outflow of urban Beijing, Atmos. Chem. Phys., 18, 9705-9721, 10.5194/acp-18-9705-2018, 2018a.
Wang, M., Chen, D., Xiao, M., Ye, Q., Stolzenburg, D., Hofbauer, V., Ye, P., Vogel, A. L., Mauldin, R. L., Amorim, A., Baccarini, A., Baumgartner, B., Brilke, S., Dada, L., Dias, A., Duplissy, J., Finkenzeller, H., Garmash, O., He, X.-C., Hoyle, C. R., Kim, C., Kvashnin, A., Lehtipalo, K., Fischer, L., Molteni, U., Petäjä, T., Pospisilova, V., Quéléver, L. L. J., Rissanen, M., Simon, M., Tauber, C., Tomé, A., Wagner, A. C., Weitz, L., Volkamer, R., Winkler, P. M., Kirkby, J., Worsnop, D. R., Kulmala, M., Baltensperger, U., Dommen, J., El-Haddad, I., and Donahue, N. M.: Photo-oxidation of Aromatic Hydrocarbons Produces Low-Volatility Organic Compounds, Environmental Science & Technology, 54, 7911-7921, 10.1021/acs.est.0c02100, 2020.
Wang, S., Riva, M., Yan, C., Ehn, M., and Wang, L.: Primary Formation of Highly Oxidized Multifunctional Products in the OH-Initiated Oxidation of Isoprene: A Combined Theoretical and Experimental Study, Environmental Science & Technology, 52, 12255-12264, 10.1021/acs.est.8b02783, 2018b.
Wang, Z., Ehn, M., Rissanen, M. P., Garmash, O., Quéléver, L., Xing, L., Monge-Palacios, M., Rantala, P., Donahue, N. M., Berndt, T., and Sarathy, S. M.: Efficient alkane oxidation under combustion engine and atmospheric conditions, Communications Chemistry, 4, 18, 10.1038/s42004-020-00445-3, 2021.
Wu, R., Vereecken, L., Tsiligiannis, E., Kang, S., Albrecht, S. R., Hantschke, L., Zhao, D., Novelli, A., Fuchs, H., Tillmann, R., Hohaus, T., Carlsson, P. T. M., Shenolikar, J., Bernard, F., Crowley, J. N., Fry, J. L., Brownwood, B., Thornton, J. A., Brown, S. S., Kiendler-Scharr, A., Wahner, A., Hallquist, M., and Mentel, T. F.: Molecular composition and volatility of multi-generation products formed from isoprene oxidation by nitrate radical, Atmos. Chem. Phys., 21, 10799-10824, 10.5194/acp-21-10799-2021, 2021.
Xu, Z. N., Nie, W., Liu, Y. L., Sun, P., Huang, D. D., Yan, C., Krechmer, J., Ye, P. L., Xu, Z., Qi, X. M., Zhu, C. J., Li, Y. Y., Wang, T. Y., Wang, L., Huang, X., Tang, R. Z., Guo, S., Xiu, G. L., Fu, Q. Y., Worsnop, D., Chi, X. G., and Ding,

A. J.: Multifunctional Products of Isoprene Oxidation in Polluted Atmosphere and Their Contribution to SOA, Geophysical Research Letters, 48, e2020GL089276, https://doi.org/10.1029/2020GL089276, 2021.
Yan, C., Nie, W., Äijälä, M., Rissanen, M. P., Canagaratna, M. R., Massoli, P., Junninen, H., Jokinen, T., Sarnela, N., Häme, S. A. K., Schobesberger, S., Canonaco, F., Yao, L., Prévôt, A. S. H., Petäjä, T., Kulmala, M., Sipilä, M., Worsnop, D. R., and Ehn, M.: Source characterization of highly oxidized multifunctional compounds in a boreal forest environment using positive matrix factorization, Atmos. Chem. Phys., 16, 12715-12731, 10.5194/acp-16-12715-2016, 2016.
Zaytsev, A., Koss, A. R., Breitenlechner, M., Krechmer, J. E., Nihill, K. J., Lim, C. Y., Rowe, J. C., Cox, J. L., Moss, J., Roscioli, J. R., Canagaratna, M. R., Worsnop, D. R., Kroll, J. H., and Keutsch, F. N.: Mechanistic study of the formation of ring-retaining and ring-opening products from the oxidation of aromatic compounds under urban atmospheric conditions, Atmos. Chem. Phys., 19, 15117-15129, 10.5194/acp-19-15117-2019, 2019.
Zhang, H., Li, H., Zhang, Q., Zhang, Y., Zhang, W., Wang, X., Bi, F., Chai, F., Gao, J., Meng, L., Yang, T., Chen, Y., Cheng, Q., and Xia, F.: Atmospheric Volatile Organic Compounds in a Typical Urban Area of Beijing: Pollution Characterization, Health Risk Assessment and Source Apportionment, Atmosphere, 8, 10.3390/atmos8030061, 2017.
Zhang, L., Li, H., Wu, Z., Zhang, W., Liu, K., Cheng, X., Zhang, Y., Li, B., and Chen, Y.: Characteristics of atmospheric volatile organic compounds in urban area of Beijing: Variations, photochemical reactivity and source apportionment, Journal of Environmental Sciences, 95, 190-200, https://doi.org/10.1016/j.jes.2020.03.023, 2020.
Zhao, D., Pullinen, I., Fuchs, H., Schrade, S., Wu, R., Acir, I. H., Tillmann, R., Rohrer, F., Wildt, J., Guo, Y., Kiendler-Scharr, A., Wahner, A., Kang, S., Vereecken, L., and Mentel, T. F.: Highly oxygenated organic molecule (HOM) formation in the isoprene oxidation by NO_3 radical, Atmos. Chem. Phys., 21, 9681-9704, 10.5194/acp-21-9681-2021, 2021.
Ziemann, P. J.: Effects of molecular structure on the chemistry of aerosol formation from the OH-radical-initiated oxidation of alkanes and alkenes, International Reviews in Physical Chemistry, 30, 161-195, 10.1080/0144235X.2010.550728, 2011.